CHARACTERIZATION OF SECONDARY MINERALS FORMING AT FRACTURE SURFACES IN AQUITARDS

by

Catherine Ann Corrigan

A thesis submitted to the
Department of Geological Sciences
in conformity with the requirements for the degree of
Master of Science

Queen's University
Kingston, Ontario, Canada,
1998

Abstract

Hydraulically-conductive fractures in aquitards control the movement of groundwater and contaminants, thus characterization of pervasive secondary mineral coatings on fracture surfaces is important to understanding contaminant transport. The major coating constituents have historically been documented simply as Fe- and Mn-oxides, but surface chemistry and, therefore, contaminant retardation, will vary depending on mineralogy, grain size and crystallinity.

Fracture coatings at two previously well-characterized field sites were studied: the Dalmeny site in southern Saskatchewan, and the Laidlaw site near Sarnia, Ontario.

At both sites, coatings vary systematically with depth and horizons were defined in order to focus more detailed investigation. SEM with EDS, petrography and electron microprobe analyses with EDS, and XRD were used for the detailed characterization.

Fe-oxide deposits are generally more laterally extensive and form the interstitial material at fracture surfaces at both locations. Goethite and possibly ferrihydrite are present, and at Dalmeny, hematite occurs locally.

In contrast, Mn-oxides form in relatively pure isolated clusters. Their exact mineralogy could not be defined, but at both locations, the Mn-oxide at more shallow depths may be vernadite ($MnO_2 \bullet nH_2O$), and at Laidlaw, todorokite ($(Ca,Na,K,)_{0.3\text{-}0.5}(Mn^{4+},Mn^{3+},Mg)_6O_{12} \bullet 3\text{-}4.5H_2O$) and rancieite ((Ca,

$Mn^{2+})Mn^{4+}{}_7O_{14}\bullet 2.8H_2o$) may be present at greater depths. Mn-minerals are about 1 μm or less in size.

At Laidlaw, silvery-grey coating material previously thought to consist of reduced Fe-minerals was identified as authigenic carbonates and aluminosilicates.

Because Fe-oxide deposits are more laterally extensive and form as cement at fracture surfaces, their presence is expected to result in a decrease in matrix permeability adjacent to the fracture. The formation of Fe-oxides at fracture surfaces, then, may impede the ability of contaminants in fractures to diffuse into the matrix. Moreover, this phenomenon will occur regardless of mineralogy.

Acknowledgements

First and foremost, I would like to thank my supervisors, Dr. Vicki Remenda and Dr. Heather Jamieson, for their support, encouragement and patience throughout the duration of this thesis. The two were a perfect complement in terms of guidance. This project has been supported financially through a grant from the Waterloo Centre for Groundwater Research and through NSERC grants to V. Remenda and H. Jamieson. Personal support was additionally provided by a Reinhardt Fellowship.

Thanks to my committee members Dr. Bernie Kueper, and Dr. Herb Helmstaedt for reviewing this thesis, and in particular to Dr. Kurt Kyser for the discussions over the years.

The success of my XRD analyses is indebted in large part to Dr. Ron Peterson, who served as an unofficial advisor where this part of my thesis was concerned. Additional thanks are owed to Aliona Valyashko and Al Grant.

Glen Kirkpatrick, at the University of Waterloo, was a huge help with field work at the Laidlaw site. Thanks also go to Scot Ridler.

SEM analyses were performed with Paul Nolan, formerly with the Department of Materials and Metallurgical Engineering, and help with electron microprobe work was provided by Dave Kempson. Rob Harrap provided much needed guidance for GIS map-making. Thanks to Roger Innes for help with the mini-mounts, and for just being such a generally helpful guy all around!

Helpful insight into the "bug" influence on coating formation was provided by Dr. Barbara Sherriff at the University of Manitoba. Thanks also to Dr. Bob McLean for his help in this area.

There are many people, who, over my extensive time spent in the Geology Department, have provided support and friendship. You have been my surrogate family and I thank you all. I also wish to thank the gang at the Grad Club and the summer of '97 "community of women" for your unfailing support in the latter stages of this thesis.

Finally, thanks to my mom, Judy Corrigan, for her unending encouragement over the years - happy retirement!

Table of Contents

List of Tables.

List of Figures

Chapter 1: Introduction

The focus of much of the research on clay-rich, unlithified aquitards has been on their increased permeability due to the presence of hydraulically-conductive fractures (e.g. McKay and Fredericia, 1995; Keller et al., 1986; Grisak and Cherry, 1975). It is these fractures that control the bulk hydraulic conductivity of the aquitard. Their presence can increase bulk aquitard permeability by several orders of magnitude above matrix permeability (McKay and Fredericia, 1995; D'Astous et al., 1989; Keller et al., 1986; Grisak et al., 1976; Grisak and Cherry, 1975) In fact, early methods for the evaluation of the hydraulic conductivity (K) of unlithified aquitards, such as laboratory consolidation tests performed on core, ignored the effects of fractures on K. Often the fractures are not discernible to the eye and, thus, their presence is unknown and their effect is not considered when measuring K (Keller et al., 1986).

One characteristic of fractures that is ubiquitous and diagnostic of their presence is secondary mineral coatings on their surfaces. Iron and Mn-oxides are frequently documented fracture coatings, with mineralogical identifications based simply on coating colours. The coatings are pervasive in the weathered zone and frequently extend below the interface between the weathered and unweathered zones (McKay and Fredericia, 1995; Ruland et al., 1991; Keller et al., 1986). Research to date has only documented their presence, and

occasionally noted the appearance of such minerals as calcite and gypsum (Klint, 1996; McKay and Fredericia, 1995; Keller et al., 1991; Hendry et al., 1986).

More recently, much research has focused on the migration of contaminants through fractured aquitards (e.g. McKay et al., 1993b; Jørgensen and Fredericia, 1992). Although coatings are the solid phase materials first encountered by contaminants in fractures, little is known of their mineralogy and chemistry. The mineralogy, surface area, and crystallinity of the coatings will affect the fracture surface chemistry and, thus, may retard groundwater contaminants. The iron and Mn-oxides, hydroxides and oxyhydroxides (henceforth referrred to collectively as Fe- or Mn-oxides) which might form in these environments would each have varying surface properties: for example, because the Fe-oxide ferrihydrite typically has poor crystallinity and forms very small, spherical grains, it has much greater surface reactivity than the other Fe-oxides (Schwertmann and Taylor, 1989).

Identification of authigenic iron and Mn-oxides has been done extensively with soils (e.g. Schwertmann and Taylor, 1989; McKenzie, 1989) and marine sediments (e.g. Burns and Burns, 1979; Murray, 1979) and less commonly with lacustrine sediments (Fortin et al., 1993), aquifer or stream grain coatings (Coston et al., 1995; Potter and Rossman, 1979b; Koljonen et al., 1976), and desert varnish (Potter and Rossman, 1979c). In all of the above settings, the primary reason for studying these minerals is due to their known adsorptive

properties (Coston et al., 1995; Carlos et al., 1993; Fortin et al., 1993; Belzile and Tessier, 1990; Cerlin and Turner, 1982; Robinson, 1982)

While the mineralogy and adsorptive properties of iron and Mn-oxides have been studied in the settings listed above, it would appear that, to date, fracture coatings in clay-rich aquitards have not been investigated. For the reasons outlined above, knowledge of coating chemistry would be valuable. Furthermore, the hydrogeochemical conditions are unique for this particular environment. Since the coating minerals are present on fracture surfaces and not throughout the matrix, clearly there must be geochemical differences in the two settings. From a strictly physical hydrogeologic perspective, flow through fractures is predominantly advective, while through the matrix, is probably exclusively diffusive. These different conditions can potentially translate into significant variations in the chemical conditions over mere centimetres, from within the fractures to within the matrix. The advective transport in fractures may allow for waters with soil-type chemistry, with more acidic pH and higher Eh, to penetrate much further into the aquitard than would be possible by diffusive transport. Furthermore, reaction time and, therefore, rate, will be different in the two regimes. The end result is that small scale chemical gradients may develop. Because of the strong dependency of Fe and Mn mineral stabilities on redox conditions (Drever, 1988) it seems likely that the dominant chemical gradient existing between the matrix and the oxide-coated fractures is one of Eh.

To characterize fracture coatings, knowledge of the specific mineralogy,

grain size and morphology, and relation of coating minerals to the matrix was sought. In addition to providing information on surface reactivity, it was anticipated that the study might provide insight into the mechanisms of fracture coating formation.

Because these types of samples have not been studied previously, techniques for mineral analyses needed to be developed, or methods used for other settings had to be modified. Studying fracture coatings presented some unique difficulties, which will be described later. Therefore, much of this paper will focus on methodology for their proper characterization.

Chapter 2: Fe-oxide Mineralogy

There are five main Fe-oxide minerals which occur authigenically in surficial environments: goethite (α-FeOOH), hematite (α-Fe_2O_3), ferrihydrite ($5Fe_2O_3 \bullet 9H_2O$), lepidocrocite (γ-FeOOH), and maghemite (γ-Fe_2O_3), where α, and γ, refer to the crystal structures hexagonal close-packed and cubic close-packed, respectively. Less commonly, akaganeite (β-FeOOH), feroxyhite (δ-FeOOH) and the ferric-ferrous hydroxide phase "green rust" are also formed (Schwertmann and Taylor, 1989).

The following table lists some of the diagnostic characteristics of the main Fe-oxides:

Table 1. Characteristics of main Fe-oxides (Schwertmann and Taylor, 1989).

Mineral	Formula	Colour (Munsell)	Crystal Morphology	d-spacings (nm)
Goethite	FeOOH	Yellowish-brown 7.5YR-2.5YR	needles, laths	0.418, 0.245, 0.269
Hematite	Fe_2O_3	Bright red 5R-2.5YR	Hexagonal plates	0.270, 0.368, 0.252
Ferrihydrite	$5Fe_2O_3 \bullet 9H_2O$ $Fe_5(O_4H_3)_3$ $Fe_5HO_8 \bullet 4H_2O$	Reddish-brown 5YR-7.5YR	spherical	0.25-0.26, 0.223,0.197, 0.17, 0.15
Lepidocrocite	FeOOH	Orange 5YR-7.5YR	laths	0.626, 0.329, 0.247,0.1937
Maghemite	Fe_2O_3	Red to brown	cubes	0.252, 0.295

While colour can be fairly diagnostic for the Fe-oxide minerals, it can be

misleading; smaller grain size will result in darker and slightly brighter shades. In addition, cation substitutions can significantly alter colour. Six mole percent Mn substitution for Fe will effectively mask the Fe-oxide characteristic colour yielding a much more greyish-green coloured mineral (Schwertmann and Cornell, 1991). Aside from cation-substitution effects, frequently Fe-oxides will occur admixed within themselves and with Mn-oxides. As little as 10 percent Mn-oxides present will effectively mask the colour of Fe-oxides (Dixon and Skinner, 1992).

Goethite is the most prevalent Fe-oxide in weathering environments and soils to which it imparts the common yellowish-brown colour. The structural unit for the Fe-oxide minerals is the octahedron of form $Fe(O, OH)_6$. With the goethite structure, the octahedra are linked into chains by Fe-O-Fe or H bonds, and cross-linked into double chains through edge sharing of slightly offset octahedra in the adjacent chains. The crystal morphology of synthetic goethite is acicular. Needle-shaped grains do occur naturally, although in soils, irregularly shaped grains are more usual (Schwertmann and Taylor, 1989; Murray, 1979). According to Norrish and Taylor (1961), Al can substitute for as much as one third of Fe in soil goethites, with degree of substitution increasing with decreasing grain size. This substitution has the effect of diminishing acicularity, and shifting XRD d-spacing peaks to lower values, with the magnitude of these changes dependent on degree of substitution (Schwertmann and Taylor, 1989).

Goethite can occur in almost any low-temperature environment. It is formed through oxidation of Fe^{2+} ions in solution, with a subsequent hydrolysis-type precipitation. It can also form from ferrihydrite through a dissolution/reprecipitation reaction. It is the stable polymorph of FeOOH to which other forms will convert (Schwertmann and Taylor, 1989).

Hematite is the second most common Fe-oxide. Its colour can vary from bright red, when particles are small or dispersed, to a more deep shade for larger grains or more dense deposits. Because of its strong pigmentation effect, only a few percent of hematite present in a deposit is required to mask the presence of other Fe-oxides. The hematite crystal structure consists of adjacent octahedra sharing faces through a slight distortion of the structural units. The resulting structure is a dense and compact, infinite, three-dimensional network of octahedra. Ideal crystal morphology is hexagonal, and this shape does often occur in samples from surficial settings (Schwertmann and Cornell, 1991; Schwertmann and Taylor, 1989; Murray, 1979). Aluminum replacement of iron does not occur with hematite to the same degree as with goethite; in syntheses experiments, Schwertmann et al. (1979) found that maximum Al substitution amounted to half of that achieved with goethite. With the substitution also came a corresponding shrinkage in unit cell dimensions, which would be manifested in d-spacings (Schwertmann and Taylor, 1989).

Hematite is a less common constituent of soils and weathered zones in cool or temperate zones, where the lower temperatures and higher activity of

water favour goethite formation . It does not precipitate directly from solution, but forms from ferrihydrite. Thus, factors that favour ferrihydrite formation also promote formation of hematite (see below) (Schwertmann and Taylor, 1989).

There has been much debate regarding the stability of goethite versus hematite (e.g. Schwertmann and Taylor, 1989; Fischer and Schwertmann, 1975; Langmuir, 1971; Berner, 1969). For the reaction

$$2\alpha\text{-}FeOOH \leftharpoondown \alpha\text{-}Fe_2O_3 + H_20$$

Berner (1969) found experimentally that the standard free energy (ΔG°_R) was slightly negative, however, these results were for fine-grained goethite. Both Ferrier (1966) and Langmuir (1971) studied the effects of surface area on free energy. In general, coarse-grained goethite is more stable than coarse-grained hematite in water at temperatures up to about 80 °C under atmospheric pressure. In nature, because goethite particles are generally smaller than those of hematite, the finer-grained goethite is unstable relative to coarser-grained hematite in most environments (Murray, 1979). The rarity of goethite *vis-a-vis* hematite in ancient deposits tends to reinforce this notion (Goss, 1987; Berner, 1969).

That goethite remains the predominant Fe-oxide in most surficial environments for long periods of time can be attributed to kinetics (Goss, 1987; Murray, 1979). In low temperature systems, goethite transforms to hematite very slowly. The actual mechanism for transformation under surficial conditions is thought to be a dissolution/reprecipitation reaction in which goethite is dissolved

and ferrihydrite is precipitated, with ferrihydrite ultimately being converted to hematite (Fischer and Schwertmann, 1975). Under elevated temperatures (200-300 °C), the phase transformation can occur through a simple topotactic dehydration reaction, in which the oxygen substructure remains unchanged (Goss, 1987).

Ferrihydrite is a common constituent in oxidizing groundwater systems and in soils. Its colour is the typical reddish brown hue of podzol B horizons. Structurally, ferrihydrite resembles hematite. It differs in that the Fe positions are partially vacant and some of the oxygen ions are replaced by water molecules. Previously, the mineral was referred to as amorphous Fe-oxide due to the typically very small (3 to 7 nm diameter) grain size and poorly developed crystallinity which did not allow for XRD identification. Crystallinity can vary considerably; for well-ordered ferrihydrite, six XRD peaks arise, but this number can drop to two for poorly crystallized material, often referred to as "proto-ferrihydrite" (Childs, 1992; Schwertmann and Taylor, 1989; Chukrov et al., 1973). When only two d-spacings arise, they are present as broad peaks at 0.26 and 0.15 nm. The next peaks to appear as crystallinity improves are 0.22-0.23, 0.17, and 0.20 consecutively (Childs, 1992). Because of its poor crystallinity and tiny grain size, the mineral has great "scavenging" abilities (Schwertmann and Taylor 1989). The tiny spherical grains result in a high surface area, while the structural disorder causes the surface to be more reactive (see below).

Ferrihydrite forms under conditions of rapid oxidation in environments rich in organic matter and/or silicate. Rapid oxidation and precipitation leads to disorder, while adsorption of silicate and organics inhibits crystal growth and transformation to a more ordered phase. Natural ferrihydrites from soil environments have been found to contain as much as nine percent Si with the higher Si content shifting the broad 0.26 nm XRD peak to as high as 0.29 nm (Childs, 1992). Through aggregation of the tiny grains, dehydration and internal rearrangement, ferrihydrite may eventually be converted to hematite. It may also be converted to goethite through dissolution and reprecipitation (Schwertmann and Taylor, 1989).

Ferrihydrite is also present in sheaths of bacteria, forming part of the biological iron storage protein ferritin (Childs, 1992; Schwertmann and Cornell, 1991). It is the Fe oxide usually formed by microbial oxidation (Chukhrov et al., 1973).

A polymorph of goethite, lepidocrocite exhibits an orange colour and can occur in many environments. However, as with other FeOOH phases, lepidocrocite will eventually convert to goethite, the more stable form. The lepidocrocite structure consists of octahedra arranged in staggered layers joined by hydrogen bonds. Lath-shaped and elongated platy crystals are typical, whether synthesized or natural (Schwertmann and Taylor, 1989; Murray, 1979). Al substitution is not common with this mineral; the presence of even minor amounts of aluminum favours the formation of goethite (Taylor and

Schwertmann, 1978). Lepidocrocite also does not appear to form in carbonate-rich environments where goethite forms instead. The presence of Fe^{2+} species in solution appears to be necessary for its formation, thus the mineral tends to form in slightly more reducing conditions than goethite (Schwertmann and Taylor, 1989).

Maghemite is a common reddish-brown mineral in soils from the tropics and subtropics, but because it forms from oxidation of magnetite, it can occur in many other settings. It is iso-structural with magnetite, and when fully oxidized, is a polymorph of hematite. The maghemite structure, consists of both octahedra and tetrahedra (FeO_4) forming a face-centered, cubic cell, with Fe^{2+} occupying only octahedral sites and Fe^{3+} distributed between octahedral and tetrahedral sites. While with magnetite, the cation sites are all occupied, with maghemite one-ninth of the sites are vacant when the mineral is fully oxidized (Murray, 1979). However, soil maghemites can contain up to 30g/kg of Fe^{2+} indicating that oxidation often does not go to completion (Taylor and Schwertmann, 1974). In addition to forming through direct oxidation of magnetite, maghemite may form through the heating of other Fe-oxides to temperatures between 300 and 425 °C in the presence of organics. Indeed, maghemite has commonly been reported in soils where there have been forest, peat or brush fires (Schwertmann and Taylor, 1989).

Akaganeite and feroxyhite are two other unstable polymorphs of goethite. The structure of akaganeite differs remarkably from that of the other Fe-oxides

and closely resembles that of the Mn-oxide todorokite. The octahedra share edges to form double chains which are, in turn, linked to other chains by corner sharing. This leads to an open tunnel structure which can accommodate water molecules and foreign anions. In fact, the presence of large foreign anions, such as Cl^- is required to stabilize the tunnel structure. Consequently, akaganeite is the common Fe-oxide that precipitates from sea water or other Cl^--rich environments (Murray, 1979).

Feroxyhite is a brown-coloured, poorly ordered mineral with Fe^{3+} cations having an ordered arrangement in the octahedral sites but with the O^{2-} and OH^- ions disordered (Murray, 1979). The mineral is thought to form from rapid oxidation of $Fe(OH)_2$ (s) under alkaline conditions, but is converted to goethite upon exposure to air (Schwertmann and Taylor, 1989; Murray, 1979).

Dark green-blue mixed Fe^{2+}-Fe^{3+} hydroxide phases have been given the generic name "green rust". They consist of double-hydroxy salts arranged in a layered structure, with the cations occupying the octahedral sites surrounded by OH^- groups. The presence of Fe^{3+} in octahedral sites gives rise to a net positive charge which is balanced by interlayer anions, such as CO_3^{2-}, Cl^-, and SO_4^{2-}. While easily synthesized in the lab under surficial conditions, the compounds are not often found in soils (Schwertmann and Taylor, 1989). Their presence has been noted in buried sediments, however, upon exposure to air, they are rapidly oxidized and presumably lost to a more stable ferric Fe-oxide phase.

While aluminum is a common replacement of iron in Fe-oxides, other

foreign ions can be incorporated into the structure because the minerals form from solution.

Substitution of manganese has been found to occur in synthetic goethites, however, the common presence of admixed Mn-oxide phases within Fe-oxide deposits has made it difficult to ascertain whether the manganese occurs in a phase of its own or as an isomorphous substitute in Fe-oxide phases (Stiers and Schwertmann, 1985).

The surface chemistry of oxides is of major importance in understanding their ability to attract contaminants in groundwater. In the presence of water, the surface cations of Mn- and Fe-oxides will complete their ligand shell with OH^- or H^+. Because of these outer hydroxyl groups, the surfaces will have a net charge due to excess or deficient H^+ ions, thereby attracting other ions. The pH value at which there is no net charge is called the point of zero charge (PZC) (McBride, 1994). At pH values below the PZC, the surface will be positively charged, while at higher pH values, will be negatively charged. The PZC for Fe-oxides, in the absence of influence from other ions in solution ranges between pH values of 7 and 9 (Borgaard, 1983b).

There are two main mechanisms which alter the PZC: ion adsorption and chemisorption. Ion adsorption occurs in order to neutralize the surface charge of the mineral grains. The ions become weakly bound to the surface by electrostatic forces. With this type of bonding, adsorption depends only on ionic charge; ions with the same charge would be attracted equally. In a

multicomponent system, the degree of adsorption of one ion over another of equal charge will be dictated by their activities in solution. Because they have relatively high PZC values in their pure state, natural Fe-oxides tend to adsorb anions. Upon adsorption of anions, however, the PZC value shifts to a lower value (Schwertmann and Taylor, 1989). Natural ferrihydrite samples, because of their high degree of silicate adsorption, have been found to have PZC values ranging from 5.3 to 7.5, while synthetic samples have a value near 8 (Schwertmann and Fechter, 1982).

With chemisorption, or specific adsorption, surface ions become covalently bonded with Fe^{3+} or O^{2-} on the surface; they are, thus, bound very tightly and the reaction tends towards irreversibility. Furthermore, this type of reaction favours strongly hydrolysing metals and particular minerals will show preference towards certain ions. The reaction is more likely to occur with poorly crystalline minerals because the structural disorder translates to more vacancies in the coordination shells of surface ions. Chemisorption is not dependent on a surface charge and may even augment a charge imbalance (Schwertmann and Taylor, 1989; McBride, 1994).

Chemisorption of divalent heavy metal cations by goethite has shown the following order of preference: Cu > Pb > Zn > Cd > Co > Ni > Mn. This order differs for hematite only with a reversal of position of Cu and Pb (Schwertmann and Taylor, 1989).

Chemisorption of phosphate by Fe-oxides has been studied extensively

because of its importance with soils. Other anions of preference include silicate, molybdate, arsenate, selenate, sulphate and organic ions (Schwertmann and Taylor, 1989). Generally, the anions of weak acids will be favoured (McKenzie, 1989).

Based on these results, then, the groundwater contaminants expected to be retarded by fracture coatings are the divalent metal cations and the anions of weak acids.

While poor crystallinity will increase the potential for chemisorption, surface area is also an important factor in considering surface reactivity. Because it typically forms tiny, spherical particles, ferrihydrite will generally have the highest surface area. Furthermore, because it is often disordered, its surface will be more favourable for chemisorption. Thus, ferrihydrite grains have a larger and more reactive surface than other Fe-oxides. The morphology and the coarser grain size of the other minerals gives them a smaller surface area (Schwertmann and Taylor, 1989). Hematite, because of its slower rate of formation, typically forms larger grains than goethite (Murray, 1979). Its surface area is likely the lowest of the Fe-oxides and would be expected to be the least reactive.

Chapter 3: Mn-oxide Mineralogy

Mn-oxide mineralogy is more complex than that of Fe-oxides because manganese can exist in three oxidation states: Mn^{2+}, Mn^{3+}, and Mn^{4+}. All of these states substitute for each other substantially, such that there is much replacement of O^{2-} with OH^- and incorporation of foreign ions within the mineral structures to maintain electrical neutrality. Indeed, certain minerals are characterized by cations other than Mn as essential structural constituents. In addition, there is a large variation in Mn-O (or OH) bond length which is subsequently reflected in crystal structure. Because of all these variations, and since many of the minerals commonly occur as admixed phases, identification is problematic, and for some minerals, crystal structure remains uncertain (McKenzie, 1989).

There are two main structural types of Mn-oxides: tunnel and layer structure. With the tunnel structure, chains of $Mn(O,OH)_6$ octahedra are linked through sharing of corners to form a framework of tunnels. Large foreign cations and/or water molecules occupy the tunnels. The layer structure consists of sheets of octahedra linked through edge-sharing, with water molecules or OH^- groups occupying the inter-layer region (McKenzie, 1989).

Table 2. Characteristics of Mn-oxides (McKenzie, 1989; Post, 1992; Burns and Burns, 1979, JCPDS cards).

Mineral	Ideal Chemical Formula	Structure	Crystal Morphology	d-spacings (nm)
hollandite	$Ba_2(Mn^{4+}, Mn^{3+})_8O_{16}$.	tunnel	laths, fibres	0.313, 0.240, .0215, 0.347
cryptomelane	$K_2(Mn^{4+}, Mn^{3+})_8O_{16}$.	tunnel	laths, fibres	0.239, 0.690, 0.490, 0.310
coronadite	$Pb_2(Mn^{4+}, Mn^{3+})_8O_{16}$.	tunnel	laths, fibres	0.310, 0.347, 0.154, 0.240
manjiroite	$Na_2(Mn^{4+}, Mn^{3+})_8O_{16}$.	tunnel	laths, fibres	0.241, 0.702, 0.314, 0.494
romanèchite	$Ba_{0.66}Mn^{4+}_{3.68}Mn^{3+}_{1.32}O_{10}\bullet 1.34H_2O$	tunnel	laths, fibres	0.241, 0.219, 0.348, 0.696
todorokite	$(Ca,Na,K)_{0.3\text{-}0.5}(Mn^{4+}, Mn^{3+},Mg)_6O_{12}\bullet 3\text{-}4.5H_2O$	tunnel	fibres, plates	0.968, 0.480, 0.133, 0.239
pyrolusite	MnO_2	chain		0.314, 0.241, 0.163, 0.213
ramsdellite	MnO_2	chain		0.407, 0.255, 0.166, 0.162
nsutite	$Mn^{4+}_{1-x}Mn^{2+}_xO_{2-2x}(OH)_{2x}$	tunnel		0.164, 0.400, 0.233, 0.242
birnessite	$(Na, Ca, Mn^{2+})Mn_7O_{14}\bullet 2.8H_2O$	layer	plates	0.727, 0.360, 0.244, 0.141
rancieite	$(Ca, Mn^{2+})Mn^{4+}_7O_{14}\bullet 2.8H_2O$	layer	plates	0.749, 0.143, 0.374, 0.246
takanelite	$(Mn^{2+},Ca)Mn^{4+}_7O_{14}\bullet 2.8H_2O$	layer	plates	0.757, 0.377, 0.234, 0.443
vernadite	$MnO_2\bullet nH_2O$	layer	leaflets,irregular plates	0.24, .014
buserite	$Na_4Mn_{14}O_{27}\bullet 9H_2O$	layer	pseudo-hexagonal plates	1.000, 0.728, 0.506, 0.347,
lithiophorite	$Al_2LiMn^{4+}_2Mn^{3+}O_6$	layer	granular, hexagonal plates	0.471, 0.237, 0.188, 0.945

The hollandite group is composed of double, edge-shared octahedral chains linked into a tunnel structure with a large foreign cation as an essential structural component. There are four minerals types defined within this group with their definition based on the dominant cation present. For hollandite, the cation is Ba, for cryptomelane, K, for coronadite, Pb, and for manjiroite, Na. However, these definitions represent end-members and natural samples usually show a range of composition in cations, or the different minerals occur as admixed phases such that specific identification of one of these minerals is unlikely. In order to balance the charges of the tunnel cations, the octahedral Mn^{4+} must be substituted by lower valence cations such as Mn^{3+}, Al^{3+}, and Mg^{2+}. Empirical evidence has determined that hollandite minerals formed in sedimentary environments will rarely substitute Fe for Mn (Post, 1992). Additionally, these minerals have been found to have striking cation-exchange capacities (Burns and Burns, 1979). The general formula for the mineral group is $(Ba, Pb, K, Na)_{0.8\text{-}1.5}(Mn^{4+}, Mn^{3+})_8O_{16}$ (Post, 1992). Crystal morphology is commonly fibrous, with the long axis oriented parallel to the tunnel. These minerals have been found in a wide range of environments including soils and sedimentary environments, and are thought to form from birnessite with a high concentration of foreign cations (Post, 1992; McKenzie, 1989; Burns and Burns, 1979).

The mineral romanechite consists of double and triple octahedral chains linked into tunnels which are slightly larger than those of the hollandite group.

The tunnels contain Ba and water molecules in a ratio of approximately 1:2, and may also have minor amounts of K, Na, Ca, and Sr. The ideal formula for romanechite is $Ba_{0.66}Mn^{4+}_{3.68}Mn^{3+}_{1.32}O_{10} \bullet 1.34H_2O$, and natural samples do not tend to deviate substantially from this formula. Similar to the hollandite minerals, Fe does not substitute substantially for Mn and is generally never present above trace levels (Post, 1992). The mineral typically consists of fibrous crystals and occurs as botroyoidal masses in oxidized zones, and commonly forms as intergrowths with hollandite group minerals (Post, 1992; McKenzie, 1989; Burns and Burns, 1979).

Todorokite is another Mn-oxide with a tunnel structure. In this case, the structure consists of triple chains of octahedra forming large tunnels. However, variable tunnel widths have been found such that the a_o crystal dimension changes as a multiple of 0.488 nm (Chukrov et al., 1978a). Post (1992) lists the generalized formula for the mineral as $(Ca,Na,K)_{0.3\text{-}0.5}(Mn^{4+},Mn^{3+},Mg)_6O_{12} \bullet 3\text{-}4.5H_2O$, however McKenzie (1989) includes Ba as another potential structural cation. It has been found to be a major phase in both surficial and marine sedimentary environments and may display acicular or platy morphology (Post, 1992). This mineral may often contain significant amounts of Ni, Co and Cu (Post, 1992; Burns and Burns, 1979), and may form from buserite whose structure has been stabilized by replacement cations (see below), or through hydration of the mineral vernadite (McKenzie, 1989).

The two minerals pyrolusite and ramsdellite, while structurally similar to

the tunnel group minerals, do not actually contain tunnels, per se. Rows of unoccupied octahedral sites in their structures give the appearance of tunnels, but will not accommodate foreign ions. Pyrolusite and ramsdellite both have the composition of MnO_2, but pyrolusite is the stable polymorph. Structurally they differ in that pyrolusite consists of single chains of MnO_6 formed through edge sharing and linked in the x and y directions by common corners, while ramsdellite has double chains joined by sharing edges in the y direction only (McKenzie, 1989).

Nsutite is a mineral whose tunnel structure consists of variable intergrowths of pyrolusite and ramsdellite. Its chemical formula is $Mn^{4+}_{1-x}Mn^{2+}_{x}O_{2-2x}(OH)_{2x}$, with x varying between approximately 0.20 and 0.45. Studies on the formation of nsutite have found that large amounts of foreign cations inhibit its formation (Mckenzie, 1989), but analyses of various samples have shown minor amounts of Na, Ca, Mg, K, Zn, Ni, Fe, Al, and Si. It forms as a replacement mineral associated with ore deposits (Zwicker et al., 1962).

Minerals with layer structures include birnessite, rancieite, takanelite, vernadite, buserite, and lithiophorite. The structure of these minerals is poorly understood and natural samples tend to be fairly disordered. Most information on structure has been derived from synthetic samples.

Birnessite (sometimes referred to as 0.7 nm manganite) consists of layers of edge-shared octahedra approximately 0.7 nm apart (McKenzie, 1989). Natural samples have been found to have the general chemical formula (Na, Ca,

Mn^{2+})Mn_7O_{14}•$2.8H_2O$, and synthetic versions have been produced with Na, Mg and K as the interlayer cation (Post, 1992). While four characteristc d-spacings are reported (Jones and Milne, 1956), the two lines at 0.70-0.73 nm and 0.35-0.36 nm present from sheet separation must be seen for clear diagnosis (Burns and Burns, 1979). All natural samples of birnessite have displayed broad x-ray peaks, therefore the crystal structure of this mineral remains poorly understood (Post, 1992). The mineral has been reported in a wide variety of environments, both terrestrial and marine, and has been found to be the chief Mn-mineral constituent of desert varnish (Potter and Rossman, 1979c). Samples typically display platey morphology (Burns and Burns, 1979). XRD results from the minerals rancieite ((Ca, Mn^{2+})$Mn^{4+}{}_7O_{14}$•$2.8H_2O$) and takanelite ((Mn^{2+},Ca)$Mn^{4+}{}_7O_{14}$•$2.8H_2O$) have suggested that these two minerals are isostructural with birnessite (Post, 1992).

Vernadite is a natural, poorly ordered mineral, generally yielding 2 broad XRD peaks at around 0.24 and 0.14 nm, and rarely, an additional one at 0.22nm (Post, 1992). In addition to their disorder, the crystals are quite tiny, with a subsequently high surface area. The mineral is commonly found in soils and marine settings (McKenzie, 1989; Burns and Burns, 1979) and is also a supergene alteration product (Betekhtin, 1937). Its chemical formula is MnO_2•nH_2O, but electron microprobe analyses have found that the mineral commonly contains minor quantities of K, Na, Mg, Ca, Ba and Fe (Chukhrov et al., 1978b). Structurally, it is believed to consist of randomly stacked birnessite

layers; the resulting morphology is leaflet in form, with smaller dimensions than birnessite flakes. The leaflets are commonly folded and curved giving a more fiber-like appearance (Burns and Burns, 1979). The mineral is thought to form by rapid oxidation of Mn^{2+} in solution, possibly through the interaction of microorganisms, while conditions favouring slower oxidation, birnessite would form instead (Chukhrov et al., 1978b). In many respects, vernadite and birnessite are similar to ferrihydrite and goethite, respectively.

Buserite is also conceived as having a structure similar to birnessite, but with additional OH^- groups or water molecules in the interlayer regions, thus giving rise to a separation of about 1 nm. Consequently, the most pronounced d-spacings are 1.01-1.02 nm and .50-.51 nm, and the mineral is sometimes referred to as 1 nm-manganite. Crystal morphology consists of pseudo-hexagonal plates, and its ideal chemical formula is $Na_4Mn_{14}O_{27} \bullet 9H_2O$ Upon dehydration, the mineral collapses forming sodium birnessite. However, the Na in buserite is frequently exchanged for other cations, and when the replacement cations are transition metals such as Cu, Ni, Zn, or Co, the structure appears more stable and does not collapse upon dehydration. These derivatives also have smaller d-spacings, closer to those of todorokite (McKenzie, 1989; Burns and Burns, 1979). However, Paterson (1981) found that the basal spacing of buserite expands to 2.56 nm when treated with dodecylammoium chloride, while the d-spacing for todorokite remains at approximately 1 nm.

Lithiophorite consists of alternating sheets of MnO_6 and $(Al, Li)(OH)_6$

octahedra, cross-linked by hydrogen bonds. Its chemical formula is $Al_2LiMn^{4+}{}_2Mn^{3+}O_6$. Lithium content is typically 0.2 to 0.3 weight percent, and transition metals such as Ni, Cu, and Co are common substitutes within the structure. The mineral usually occurs as masses of fine grains, but has been reported to form large (up to 1-2 cm) hexagonal plates. It is a common constituent of weathered zones and some acid soils, and has also been found in low-temperature hydrothermal veins (Post, 1992). It is thought that lithiophorite forms through alteration of birnessite (McKenzie, 1989).

The minerals manganite and hausmannite are termed lower oxides because the main Mn valence is less than 4. Manganite is the stable polymorph of MnOOH. Its structure is similar to pyrolusite, but the exchange of OH^- groups for O^{2-} results in significant hydrogen bonding between the OH^- groups of edge-shared octahedra in one chain and the corner-shared oxygens in the adjacent chains (McKenzie, 1989; Burns and Burns, 1979). In marine sediments, manganite has been found to replace Mn-bearing carbonates and silicates and may also transform to pyrolusite (Burns and Burns, 1979).

The hausmannite structure consists of alternating layers of octahedra and tetrahedra (normal spinel structure), with Mn^{2+} occupying tetrahedral sites and Mn^{3+} in octahedral sites. Both of these minerals are formed through rapid oxidation under alkaline conditions, while under acidic conditions, the higher oxides are more likely to form (McKenzie, 1989).

The PZC for the Mn-oxides are lower than those of the Fe-oxides. The

points range from a pH value of 1.5 for birnessite to 4.6 for the hollandite group (Healy et al., 1966), consequently the Mn-oxides have very high negative surface charges in typical groundwater environments and, thus, tend to adsorb cations. Furthermore, their structures are such that foreign ions can easily be accommodated.

Chemisorption is extensive on all of the Mn-oxides and does not vary with their PZC values. Studies of specific adsorption of divalent heavy metal cations has yielded the following order of preference: Pb > Cu > Mn > Co > Zn > Ni (McKenzie, 1989). Because of their highly variable compositions and the large extent of cation substitutions within the mineral structures, the degree of chemisorption occurring with Mn-oxides is ostensibly much greater than with Fe-oxides. It follows that the groundwater contaminants expected to be retarded by Mn-oxides on fracture coatings are the metal cations listed above.

Chapter 4: Field Sites

In order to study fracture coatings, field sites were sought that had previously been well characterized in terms of physical hydrogeology and hydrogeochemistry. To provide a broader perspective, it was desirable to have field sites with different geologic and hydrogeologic conditions. Figure 1 indicates the location of both field sites.

Dalmeny

The Dalmeny site lies northwest of Saskatoon in southern Saskatchewan and has also been well-described previously (e.g. Remenda, 1993; Keller et al.,1991; 1986; Fortin et al., 1991; Keller and van der Kamp, 1988). The aquitard comprises 18.5 m of till from which two units can be distinguished. The Battleford Formation, occurring in the upper 1-2 m, is highly weathered and fractured, and hydrogeologically insignificant at the site as it lies above the water table. Below this till unit lies the Floral Formation. The Floral Formation consists of a till aquitard in the upper 16-17 m underlain by 18 m of stratified drift forming an aquifer (Fortin et al., 1991; Keller et al., 1986). Both units belong to the Saskatoon Group, a regional Pleistocene deposit, and are thought to have been deposited 15 000 - 20 000 years ago, and 38 000 years ago, respectively (Christiansen, 1968). Final deglaciation of the area occurred about 11,500 before present (Christiansen, 1979).

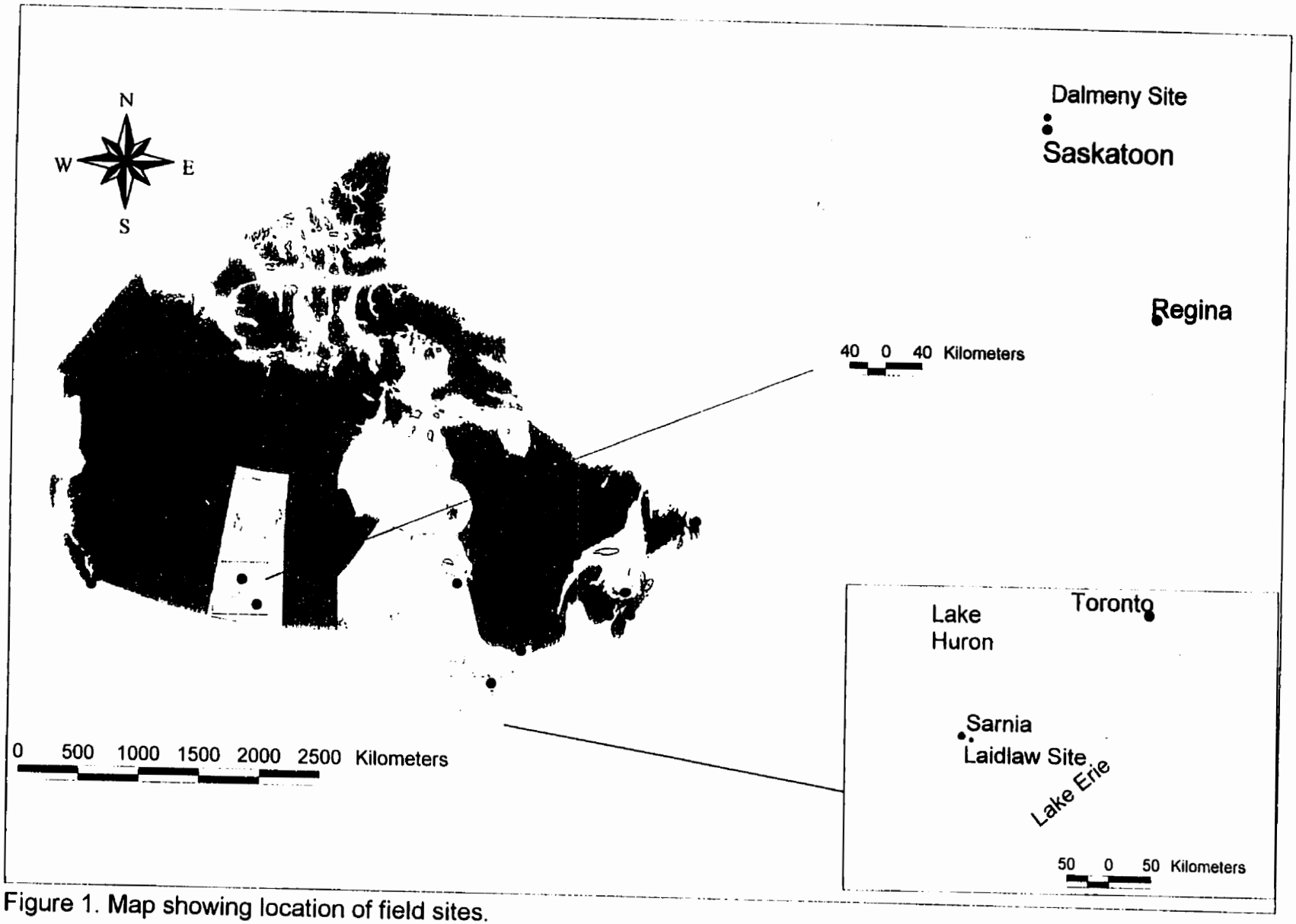

Figure 1. Map showing location of field sites.

Keller et al. (1986) found that bulk hydraulic conductivity at the site is approximately 5×10^{-9} m/s, compared to 3.5×10^{-11} m/s for unweathered till matrix. This bulk value applies to both unweathered and weathered till, indicating that the unit is fractured throughout its entire extent.

Subtle topographic depressions (5-50 cm) in the flat landscape of the area have been found to influence recharge rate and till geochemistry. The position of the water table and the gradient vary at the site according to these minor topographic variations. In the depressions, the water table occurs at approximately 4 m below surface, and the vertical component of the gradient has a value of 0.2 upwards, thereby inducing downward flow. In the higher areas, the water table position is about 7 m below surface, and the vertical component of the gradient is 0.02 upwards (Keller et al., 1988). Thus, recharge to the underlying aquifer is focused through these minor depressions leading to chemically "leached" and "unleached" areas in the till. The weathered zone extends the deepest in the unleached zone, up to approximately 10-12 m depth. In these areas, gypsum and calcite crystals commonly occur on fracture surfaces. Gypsum is not present in the leached zones. However, in both settings, oxide fracture coatings occur throughout the weathered zone and often persist up to a few metres into the unweathered zone (Keller et al., 1986, 1991).

By x-ray diffraction, Keller et al. (1991) determined that bulk weathered till mineralogy consists largely of quartz, illite, dolomite and plagioclase, with significant amounts of calcite and K-feldspar, and minor trichlorite and mixed-

layer clay.

Laidlaw

The Laidlaw site, the location of a hazardous waste treatment and disposal facility, is located 12 km south of Sarnia in southwestern Ontario. The geology and hydrogeology of the area surrounding the landfill sits has previously been detailed by Klint (1996), McKay and Fredericia (1995), McKay (1991), Balfour (1991), Ruland et al. (1991), D'Astous et al., (1989), and Desaulnier (1986). Approximately 40 m of clay-rich, glacial deposits overlie bedrock at the site. Two units have been identified: the St. Joseph Till, occuring at surface to a depth of 15-17 m, and the Black Shale Till lying below. The units are distinguished by the proportion of shale pebbles in the till, with the Black Shale Till named on the basis of its high shale content. Detailed stratigraphy and mapping by Klint (1996) has indicated that the St. Joseph Till is, in fact, a glacio-lacustrine deposit rather than till. The series of proglacial lakes formed during the final glacial retreat in the area are thought to have drained approximately 12, 000 years before present (Dreimanis, 1964).

The underlying bedrock is an aquitard consisting of the upper Devonian Kettle Point Shale, with a thin gravelly deposit occurring at the interface between the bedrock and the glacial deposits (McKay and Fredericia, 1995). The vertical component of the hydraulic gradient between the water table, the position of which varies from near surface to an approximate depth of 2 m (McKay and Fredericia, 1995), and the gravelly interface is 0.01-0.14 upwards (Richards et

al., 1984).

The weathered zone extends to 3 m below surface while fracture coatings occur typically to a depth of 4 m, occasionally extending up to 7 m (Klint, 1996). The deposit is highly fractured at surface, with fracture intensity decreasing with depth. However, below the zone of fracture coatings, fractures are not visible and their occurrence must determined indirectly. Using tritium as a tracer, the presence of which indicates post-1950 recharge, and taking water samples from standpipe piezometers at 12 locations in the area, Ruland et al. (1991) concluded that the maximum depth of hydraulically-conductive fractures in the locality varied from 7 to 13 m. The one measurement from the Laidlaw site showed detectable tritium at a depth of 7.5 m, suggesting that hydraulically-conductive fractures extend until at least that depth at the site. Hydraulic conductivity measurements vary from 3×10^{-7} m/s to 4×10^{-11} m/s, the latter of which is taken from laboratory consolidation tests and thought to represent the unfractured medium (McKay et al., 1993a).

Unweathered matrix mineralogy includes a high proportion of quartz and feldspar (40%), carbonate (35%), and clays consisting of smectite and vermiculite (2%), Fe-chlorite (10%) and illite (14%). In the weathered zone, the carbonate has been leached away and much of the chlorite has been altered to smectite (Quigley and Ogunbadejo, 1973). In the unweathered zone, this change in clay mineralogy has also been documented between fracture surfaces and the matrix (McKay, 1991). From 0.8 to 1.5 m depth, McKay (1991) noted the

presence of calcite streaks occurring along intersections of vertical fractures.

Chapter 5: Sampling and Handling

Dalmeny

Samples were obtained by augering to the desired depth, reeming out the borehole, and pushing a 7.6 cm diameter Shelby tube into the till to retrieve a core sample. The core was then extruded on site, cleaned, and archived for various purposes. Core samples from four boreholes were used for this study and these samples were air dried. Till from both leached and unleached settings was examined.

Laidlaw

Previous documentation of colour changes in fracture coatings and depth of their extent has been documented by Klint (1996). Based on this information and communication with other researchers at the site (Glen Kirkpatrick and Scott Fidler, University of Waterloo, personal communication), drilling was not necessary to reach the required sampling depth. Sampling was accomplished by excavating a trench on the north side of the Laidlaw property outside of the landfill. Trenching was done by backhoe to three different benches, from depths of 1.1 to 4.3 m below surface. The smearing from the walls of the trench was removed by knives, and sixteen intact pieces of sediment, varying in size from 30 cm (longest dimension) to 10 cm were then cut from the trench walls. The samples were chosen to be as representative as possible of the horizons present at the site. In addition to these samples, core taken by Kirkpatrick (in

progress) was examined to verify that coating variations were indeed represented by the samples taken.

Prior to and after air-drying, the till matrix and coatings were described using a Munsell Soil Colour Chart. A photographic record of the samples was made as they were air-dried to ensure that no phase changes occurred (as far as could be discerned by colour) while drying.

Chapter 6: Methods and Results

While coatings often appear as distinct "crusts" formed on top of matrix minerals, in reality they do not occur as discrete phases on their own. As mentioned previously, Fe and Mn minerals typically form as admixed phases, and other minerals, such as carbonates, which commonly precipitate from solution, may also be admixed. Furthermore, because the minerals typically form in pore spaces (Schwertmann and Fitzpatrick, 1992), they may be mixed in with matrix minerals.

Isolating coating minerals to allow for identification is, therefore, problematic. While separation techniques have been developed for some of the other settings where Fe and Mn oxides have been studied, most of these are not effective for fracture coatings. Because almost all sediment grains and coating minerals are clay-sized, separation based on grain size, as has been accomplished for films on quartz grains in aquifers or other coarse-grained sediments (e.g. Koljonen et al., 1976) does not work.

Similar to the situation with soils and marine or lacustrine sediments, the minerals are intimately associated with, and minor in quantity compared to, matrix minerals (Fortin et al., 1993). For these situations, such techniques such as selective dissolution and differential XRD, or selective dissolution combined with any other analytical technique such as Mössbauer or IR spectroscopy have proven effective (Fortin et al., 1993; Dixon and Skinner, 1992; Schwertmann et

al., 1982; Schulze, 1981; Potter and Rossman, 1979a; 1979b; 1979c). However, because the coatings vary with depth and are quite thin, obtaining adequate sample volume to perform differential solution in combination with one of the above analytical techniques is not feasible, particularly with core samples.

With these problems in mind, the following techniques were employed: 1) careful visual examination of coatings over depth and definition of coatings horizons, 2) petrographic and electron microprobe analyses with quantitative energy dispersive spectrometry (EDS) of thin sections and mini-mounts, 2) scanning electron microscopy (SEM) with qualitative EDS, and 3) x-ray diffraction (XRD). It should be noted that these techniques were most successful when used consecutively; the information provided by one often lead to a refinement in approach and guided the choice of what method to employ subsequently. The methods are presented in the recommended order of execution. Tables 3 and 4 list the samples for each technique.

Furthermore, it should be acknowledged that, although the samples were chosen to be as representative as possible, spatial variability exists within the sediments and therefore the coatings. Because of this, results should be recognized as generalizations, particularly in the case of the core samples.

Table 3. Summary of samples from the Dalmeny site. The notation D46-3, for example, indicates a sample from borehole 46, approximately 3 m below surface (exact depth interval is listed for the core samples). Position of water table is denoted by ▼ and depth to which a horizon occurs is indicated by ↓. Within the core intervals, smaller scale samples (e.g. D46-3-1) were taken for petrography, SEM and XRD analyses and these samples are listed according to borehole, general sample depth and sample number. Unless indicated otherwise, XRD analyses refer to Fe-oxide coatings.

Coating horizon	Core Samples (m from surface)	Petro-graphy	SEM and EDS	XRD
Horizon 1 ↓ 3 m	D50-1 (1.5-1.9 m) D51-1 (1.49-1.78 m)	D50-1-1		
Horizon 2 ▼ ~4 m (leached) ↓ 5 m	D46-3 (3.01-3.37 m) D46-4 (4.58-4.98 m) D50-3 (3.04-3.61 m) D50-5 (4.65-5.07 m) D51-3 (3.16-3.62 m) D51-4 (4.52-4.94 m)	D46-3-1 D46-4-1 D50-3-1	D50-3	D46-4-1 pore D46-4-2 pore D46-4-3 D51-3-1 D51-3-3 D51-3-1 Mn
Horizon 3 ▼ ~7 m (unleached) ↓ End of weathered zone (leached:8-9 m unleached: 10-12 m)	D45-5 (5.4-5.92 m) D45-6 (5.98-6.46 m) D46-6 (6.28-6.57 m) D50-6 (6.30-6.58 m) D51-6 (6.06-6.44 m)	D45-6-1 D45-6-2 D46-6-1 D50-6-1	D45-5 D45-6	D45-5-1 matrix D45-5-1 D45-5* D45-5 matrix* D45-5-2 D45-6-1 D45-6-2 D45-6-3
Horizon 4 ↓ up to a few metres	D45 10.16-10.67 m			D45-10-1 D45-10-2

*indicates samples analysed with the powder diffractometer

Table 4. Summary of samples from the Laidlaw site. The designation 3C, for example, refers to sample C from the third bench. No samples are listed as being from a second bench because more shallow samples could be more easily taken from the third bench. As above, position of water table is denoted by ▼ and depth to which a horizon occurs is indicated by ı."GM" refers to grey material and "hor" to horizon.

Coating horizon	Sediment Samples	Petrography and EDS	SEM and EDS	XRD
Horizon 1	1A, 1B, 1C, 1D, 1E, 1F ~1-1.5 m			
▼ ~2 m Horizon 2	3A, 3C, 3I ~3 m		3C-A 3I-A	GM 3I-1 GM 3I -2 Matrix GM-short* GM-long* Matrix-short* Matrix-long*
Horizon 3 ı End of weathered zone (~3 m)	3B, 3C ~3 m		3C-A 3C-B	Mn 3C-1 Mn 3C-2 LFehalo-1 LMnhor-1
Horizon 4 ı 4-7 m	3I ~3 m 3D, 3E, 3F, 3G, 3H, 3J ~4.25 m	LFe-1 LFe-2	3E-A 3E-B	Fe 3D-1 Fehor-1 Mn-Fehor-1 Mn-Fehor-2

* indicates samples analysed with the powder diffractometer, with "short" and "long" referring to the range of the scans.

1) Definition of coatings horizons:

In the initial stages, distinguishing authigenic minerals in surficial settings began with differentiation based on colour. Mn-oxides can be separated from Fe-oxides and other admixed phases based on their dark colour (Dixon and

Skinner, 1992). Distinction between the various Fe-oxides can often be performed at this stage; in its pure phase, each mineral has a fairly diagnostic colour, defined according to Munsell Soil Colour Charts (Schwertmann and Cornell, 1991; Schwertmann and Taylor, 1989). However, this stage is purely qualitative because, as described earlier, colour is affected by cation substitution, and grain size and distribution dictate brightness of colour (smaller, more dispersed grains result in brighter colour). The stronger pigmenting effect of the Mn-oxides and hematite can also mask the appearance of other minerals (Dixon and Skinner, 1992; Schwertmann and Cornell, 1991; Schwertmann and Taylor, 1989).

No documentation of any variations in Fe and Mn-mineral coatings existed for Dalmeny. Therefore, the initial stage of this study began with visual examination of the coatings for spatial variation. Examination of core from leached and unleached settings showed minimal lateral variation, while consistent variations in colour were evident over depth. Calcite and gypsum were readily identified at this stage; calcite was recognized by treatment with dilute hydrochloric acid and gypsum by its needle-like morphology. These minerals had also been documented previously by Keller et al. (1991).

With the Laidlaw site, documentation of colour variations in fracture coatings with depth had been performed previously by Klint (1996). Examination of samples indicated that, in addition to the previously documented colour variations, consistent changes in coating thickness and degree of development

also existed.

Due to these variations at both sites, it was necessary to define intervals or horizons over which to examine the coatings at a smaller scale.

Dalmeny

Four coating horizons were defined at the Dalmeny site (Fig. 2):

1) The upper horizon consists of highly weathered till with calcite (+/- gypsum), and an Fe-oxide coating of pale, rusty brown (Munsell colour 7.5YR 6-7/8) and occasional bright spots (5YR 5-6/8). Typically this horizon occurs in the upper 2 to 3 metres.

2) The second horizon is characterized by more yellowish-brown (10YR 6-7/4-6) Fe-oxide coatings and frequent dark brown (10YR 3/1) Mn-oxide mottles, again with occasional bright spots (5YR 5-6/8), occurring over a depth interval of approximately 3-5 m.

3) With the third horizon, the coatings become a rustier colour again, but are generally darker than in the first horizon, but somewhat variable in brightness and colour saturation (5YR 5/8 3-4/4-6). The Mn-oxides are a minor component and are present as small black spots. This horizon is typically present until the bottom of the weathered zone.

4) The final horizon is defined on the basis of bright rusty brown Fe-oxide coatings (7.5YR 5-6/8), no Mn-oxides and an unweathered till matrix. This horizon can extend up to a few metres below the weathered-unweathered zone interface.

Figure 2. Samples displaying representative coatings of Dalmeny horizons: A) Upper horizon of highly weathered till with calcite (+/- gypsum) and an Fe-oxide coating of pale, rusty brown (Munsell colour 7.5YR 6-7/8) and occasional bright spots (5YR 5-6/8); B) Second horizon with more yellowish brown (10YR 6-7/4-6), frequent dark brown (10YR 3/1) Mn-oxide mottles and occasional bright spots (5YR 5-6/8); C) Third horizon with darker, rusty brown (5YR 5/8 3-4/4-6) Fe-oxides and minor black Mn-oxide spots; and D) Fourth horizon of bright, rusty brown (7.5YR 5-6/8) Fe-oxides and unweathered till matrix. Note: notation on green card indicates depth from which sample was taken.

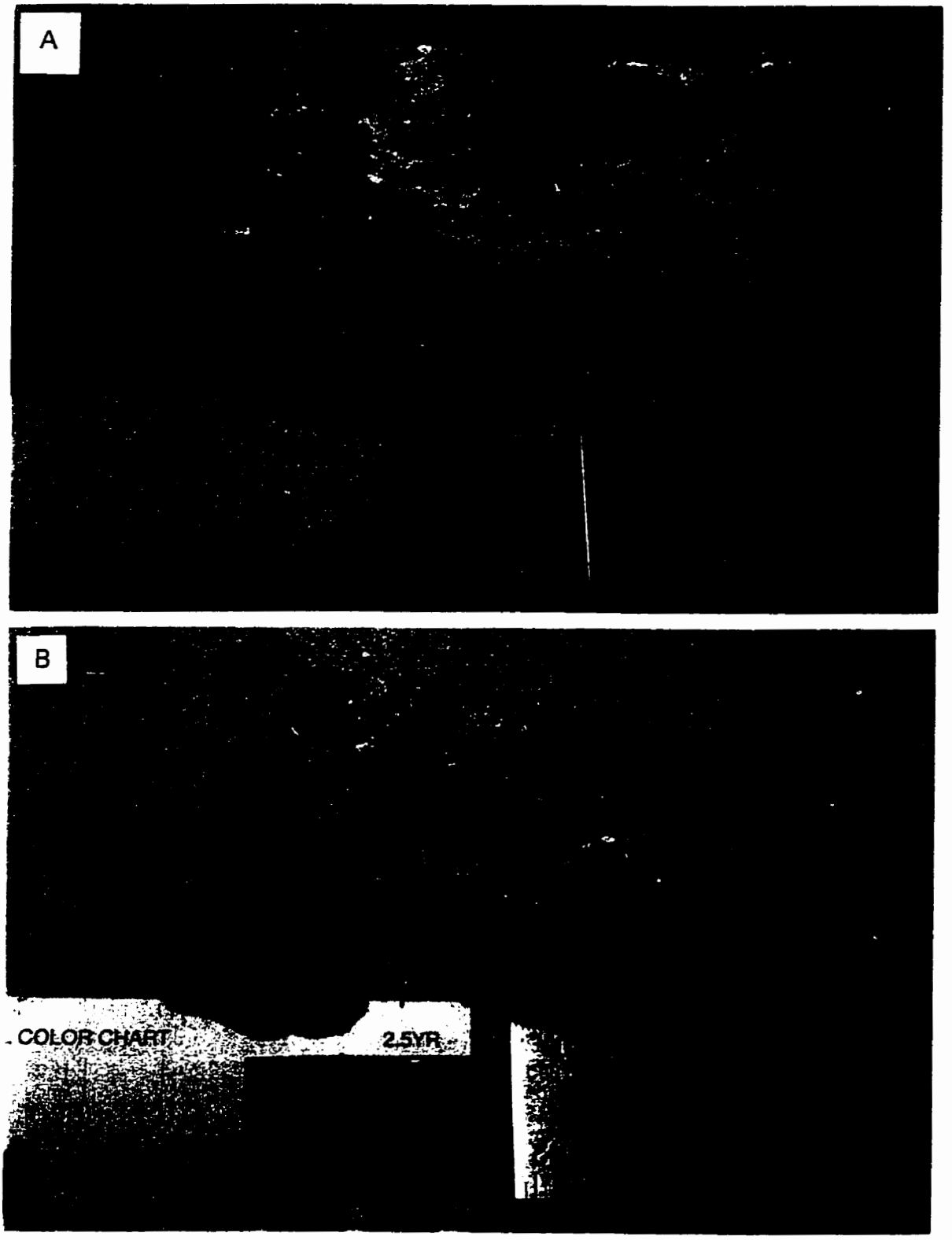
A
B
COLOR CHART
2.5YR

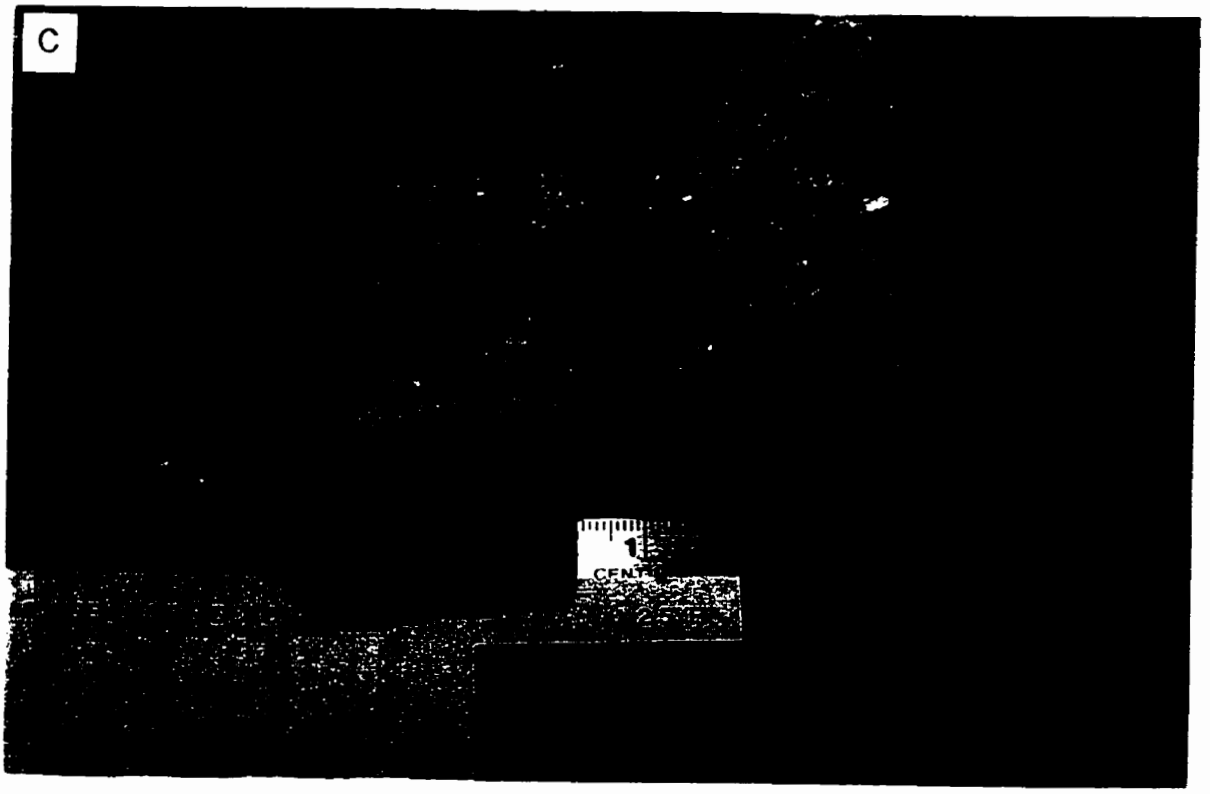
C

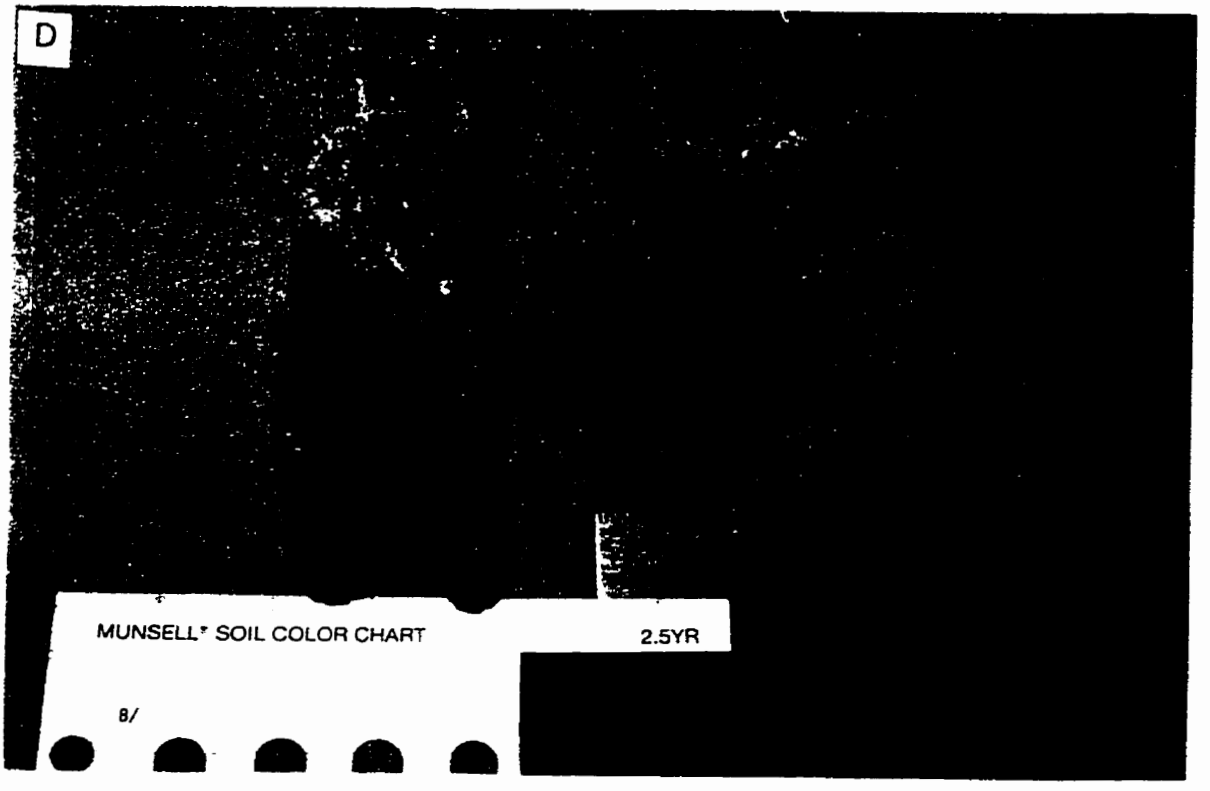
D
MUNSELL® SOIL COLOR CHART
2.5YR

Because of the overall yellowish brown colour of the second horizon, it would seem that goethite is the dominant mineral of this horizon, with little influence from the brighter minerals such as ferrihydrite and hematite. Indeed, it is likely that almost no hematite is present here since only a few percent of it will impart a reddish colour to the sediments. The more yellowish colour suggests acicular, μm-sized grains (Schwertmann and Cornell, 1991). The paleness may be indicative of more dispersed minerals. However, the occasional brighter spots do suggest hematite and/or ferrihydrite is present in these limited areas.

The rusty hue of the other horizons suggests an influence from one of the other more pigmenting minerals. Based on the characteristic colours of each of the minerals however (table 1), the coatings are likely a mixture of different Fe-oxides. The change in brightness over depth is indicative of a change in Fe-oxide grain size, with the fourth horizon characterized by the smallest particles, and the third with the largest.

With all of the horizons, the coatings appear to occur only at the surface and do not visibly penetrate into the matrix.

It should be noted that it was not expected to find lepidocrocite in this environment because of the high carbonate content of both the till and the water (Schwertmann and Taylor, 1989). Typical water analyses taken from depths ranging from 2.6 m to 14.6 m below surface have yielded HCO_3^- concentrations varying from 7.4 to 12.0 mmol/L (average=10 mmol/L) in the leached settings, and 5.7 to 15.2 mmol/L (average=12 mmol/L) in the unleached areas. Log P_{CO2}

values ranged from -1.0 to -1.9 (Keller et al., 1991). In carbonate-rich environments goethite usually forms instead of lepidocrocite (Schwertmann and Taylor, 1989).

Laidlaw

Four horizons are also defined at the Laidlaw site (Fig. 3):

1) The upper horizon consists of highly weathered till with bright white, slightly pinkish calcite streaks (2.5YR 8/2) and a whitish-grey material (2 gley 8/5B).

2) The second horizon is characterized by silvery-grey (1 gley, 8-7/N-10Y) material haloed by brownish-yellow (10YR 7-6/6) Fe-oxides. The coatings are fairly thick here and very well developed.

3) The third horizon is quite variable. In some locations it occurs as a thin (1-2 cm) interface of Mn-oxide mottles between the second and fourth horizon. Alternatively, it can be quite extensive in depth (close to a metre), consisting of mottles and dendrites of Mn-oxides, dark grey to black in colour, with the non-oxide phase present as background.

4) The final horizon is defined by its characteristic bright rusty brown Fe-oxide coatings. The coatings are fairly uniform in colour, suggesting that the same minerals are present throughout. Minor Mn-oxides are also present in this zone as small black mottles.

The coatings at Laidlaw differ from those at Dalmeny in that the variation in colour (and presumably mineralogy) not only occurs with depth, but also

Figure 3. Samples displaying representative coatings of Laidlaw horizons: A) Upper horizon of highly weathered till with bright white calcite streaks (2.5YR 8/2) and a whitish grey material (2 gley 8/5B); B) Second horizon of silvery-grey material (1 gley, 8-7/N-10Y) grading into third horizon; C) Third horizon of sooty, dark grey Mn-oxide dendrites; and D) Fourth horizon of bright rusty brown Fe-oxide with transition zone of Mn-oxides from third horizon and silvery material of second horizon. Note: notation on white cards indicates depth from which samples were taken. B was taken from the same depth as C.

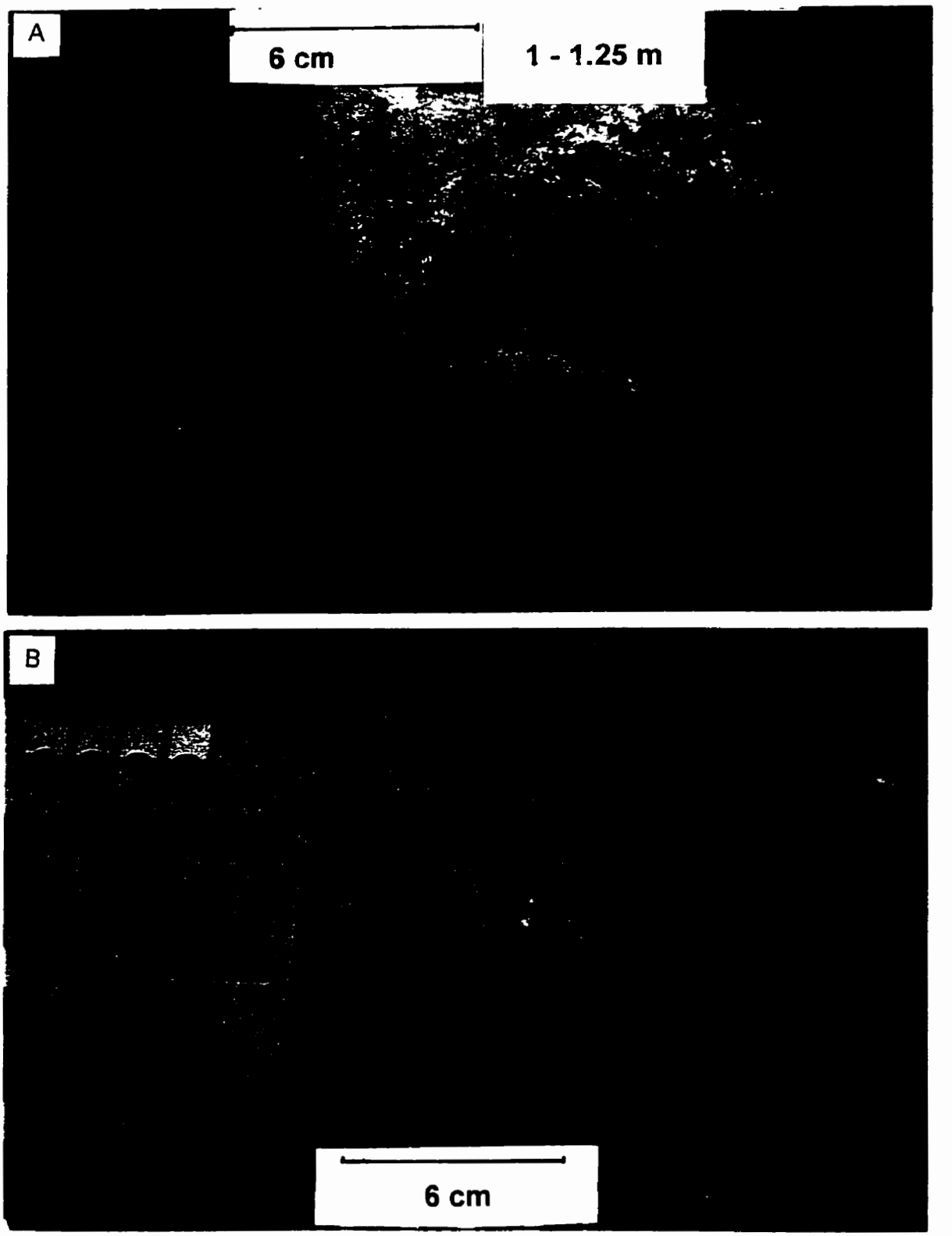
A
6 cm
1 - 1.25 m
B
6 cm

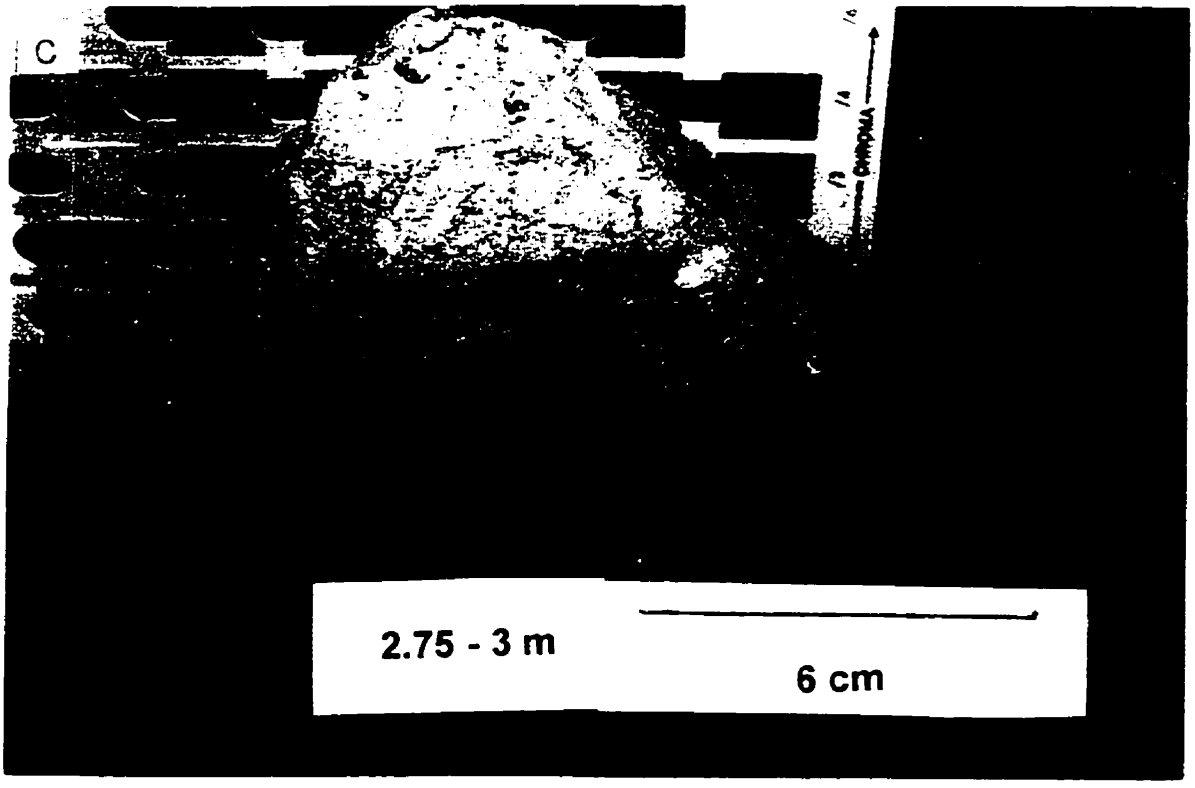
C
2.75 - 3 m
6 cm

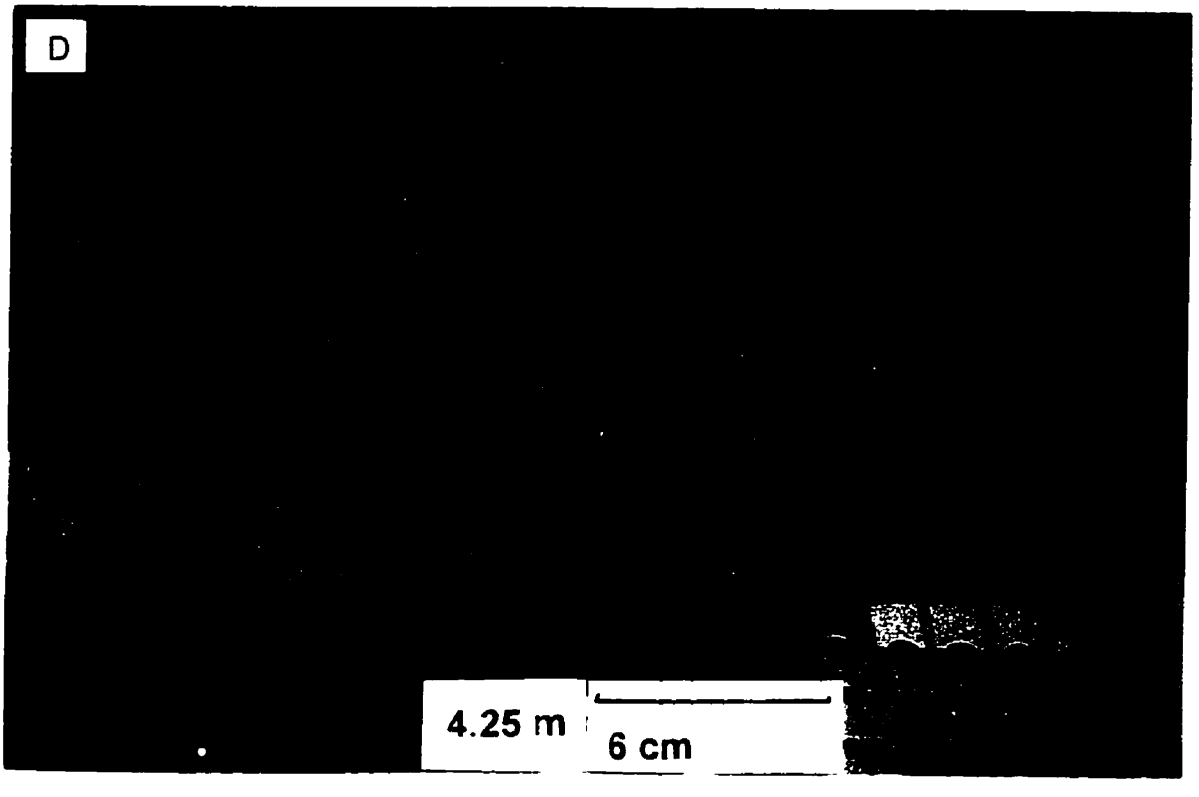
D
4.25 m
6 cm

inward from the fracture surfaces. It is also not possible to define horizons as occurring over specific depth intervals, because at some depths all horizons may be present. The variability of fracture density, size and hydraulic activity at Laidlaw results in changeable horizon depths. For example, in the major fractures, which typically run the deepest, the first horizon may persist to much greater depths than in smaller ones, while in small, discontinuous cracks, the fourth horizon might be the only one present. Because the hydraulic conductivity at Dalmeny is more consistent with depth, it seems reasonable to assume that the fracture network remains the same, and therefore coatings vary more systematically with depth. However, examination of coatings with core limits the observations of lateral variations due to changes in fractures.

At both sites, the sediments from the first horizon are weathered quite uniformly throughout. For these reasons, coatings are not well-developed and, thus, not very significant, from hydrogeologic and chemical perspectives. With the exception of one thin section made from Dalmeny, the first horizons were not further examined in this study.

2) Petrography

Thin sections were made of till and coatings from the Dalmeny site by Vancouver Petrographics Ltd. To guard against phase changes or losses, the sections were cold-impregnated, ground in oil and cold-mounted with kerosene.

Weathered till matrix minerals identified include quartz, plagioclase,

microcline, carbonates, and chlorite. In transmitted light, coatings generally appear as dark, semi-opaque, rusty sludge covering matrix minerals, or surrounding larger grains and large pores or cracks. In some places, the material becomes darker and more opaque, occasionally forming more distinct grains. Under reflected light, goethite could be identified based on internal reflections (Fig. 4). Where the coatings did not form distinct grains, the overall coating material glowed the bright yellow colour of goethite internal reflections, despite the fact that the only distinct grains visible were those of the matrix. In this manner, goethite was identified in the first, second and third horizons at Dalmeny.

In the weathered till, occasional, tiny reflective grains were present. These grains were too small to be identified under the microscope. In the unweathered till, the groundmass was quite "sparkly" and there were more tiny, reflective grains.

Under the electron microprobe, some of the reflective grains were identified as ilmenite, and others as pyrite. The sparkly appearance of the unweathered till matrix was attributed to pyrite. Keller and van der Kamp (1988) found that total sulphur content in unoxidized till was approximately 2000 to 2500 µg/g, of which the majority of the sulphur was in reduced form and deemed to be inorganic sulphides because of the low (0.5%) total organic content of the unoxidized till. These sulphur values would translate to a pyrite concentration of approximately 7.5 to 9.4 mg/g in the till. In addition to these tiny pyrite grains,

Figure 4. Photo micrographs of Dalmeny coating: A) Coating in reflected light. The brighter, more reflective white specks in A are the Fe-oxides and the bright yellow mass in A is due to goethite internal reflections; B) Coating in transmitted light. The overall yellowish colour and the darker brown and rusty masses are the Fe-oxides coatings. The rustier mass is goethite, based on the internal reflections of A.
The long dimension of the photo is 9.5 mm.

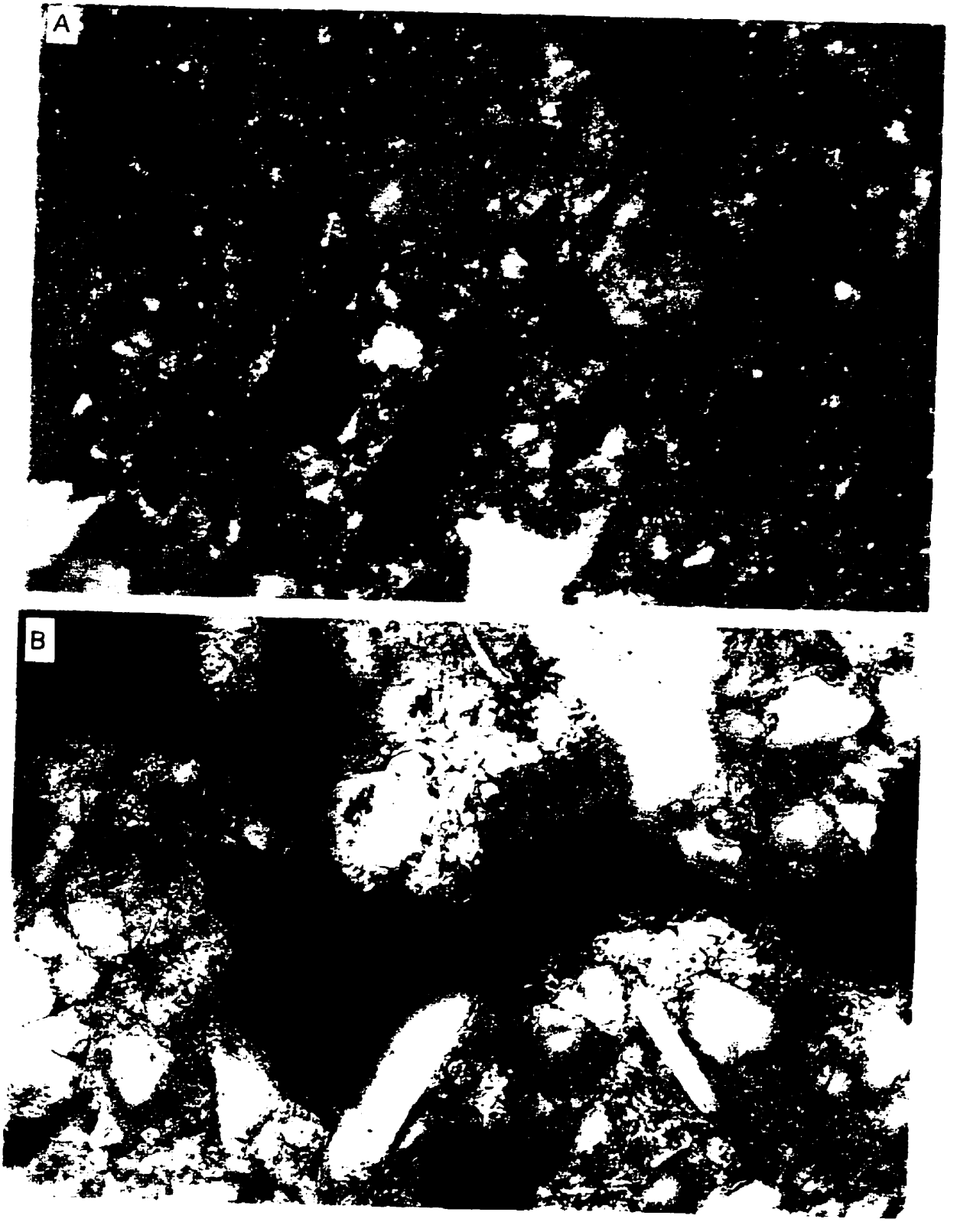
A
B

some larger grains weathering to goethite were also observed.

While the thin sections were useful for verifying matrix minerals and allowed for a closer view of coating formation, the resolution was not adequate to fully characterize fracture coating minerals. Furthermore, because the fracture coating surfaces are fairly irregular, cutting sections with much of the actual coating featured proved problematic.

Production of thin sections was attempted for samples from the Laidlaw site but a suitable epoxy could not be found to cement the sediments to allow for cutting and grinding.

Mini-mounts were made of coatings from the Fe-rich horizon at Laidlaw. Areas that appeared as a coherent crust under a binocular microscope were chipped off and the flakes were poured into a small glass tube closed off at the bottom by cellophane. The tubes were backfilled with cold epoxy and allowed to set for 24 hours. The tape was then removed and the bottom surface, exposing the sample, was ground and polished with diamond paste.

Inspection of the samples under reflected light allowed for identification of goethite, again based on bright yellow internal reflections. As with the thin sections from Dalmeny, distinct goethite grains were not visible but the overall matrix glowed a bright yellow. In one sample, a small, more reflective area with concentric banding was observed (Fig. 5).

Analyses of the mini-mount samples were performed with an ARL-SEMQ electron microprobe and quantitative EDS, using an accelerating voltage of 15

KV and a beam current of 40 nAmps. A basaltic glass standard (Queen's internal standard S-204) was used in conjunction with magnetite and Mn_2O_3 standards run as unknowns. With these standards, all Fe is assumed to be Fe^{2+} and all Mn is assumed to be Mn^{2+}. A refit was performed for the Mn_2O_3 standard such that the measured weight percent total was 93.16 percent, with the actual total at 92.26 percent. The total from the magnetite standard was measured as 93.62 weight percent which is close to the actual value of 93 percent.

Back-scattered electron (BSE) images were also examined during microprobe analysis. "Well-coated" areas appeared as slightly brighter regions in the images (indicating the presence of elements with a higher average atomic number than the adjacent areas) with matrix minerals clearly visible. EDS analyses yielded a typical spectrum for the matrix minerals but with a high Fe peak in addition. The edges of the sample flakes often appeared brighter and EDS analyses confirmed the presence of more Fe in these regions (Fig. 6). It is surmised that because the samples were flaked off, the edges might be thinner than the centre, thereby decreasing the amount of matrix material plucked up with the coating and increasing the purity of the coating material. This results in the brighter, and more Fe-rich edges.

Figure 5. Photo micrographs of coatings from the Laidlaw fourth horizon: A) the overall bright yellow colour is due to the internal reflections of tiny goethite grains surrounding larger matrix minerals; and B) the banded area starting near the left hand side of the photo is an Mn-oxide whose composition is listed in Table 3.
The long dimension of the photos is 330 μm.

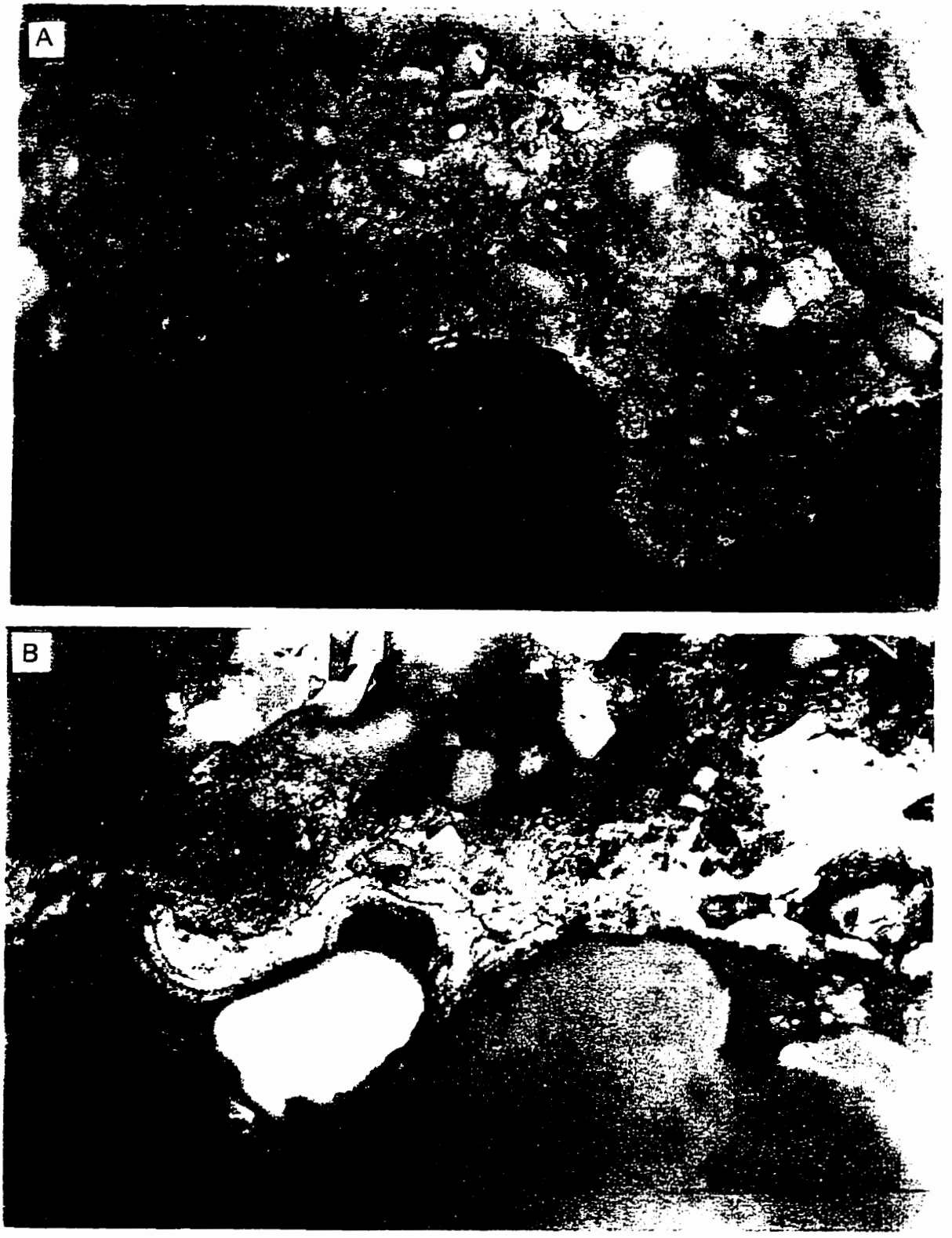
A
B

Examination of Fe-rich coating material microscopically and in BSE images provided a clear understanding of the relationship of coating minerals to the matrix. Fe-oxides are forming in the interstitial areas of the sediments and as coatings around the existing matrix grains. They are not forming as a distinct layer on the fracture surfaces. Thus, the Fe-oxides are, more accurately, a cement rather than a coating.

Quantitative analyses of the banded area demonstrated that it is an Mn-oxide with significant amounts of Fe, Ca, Al and Mg, and minor Si, Ti, Na, K, S and Cl (table 5). It should be noted that the Ti peak may be Ba. The main peaks of these two elements are very close and, because the standard contained Ti and not Ba, the quantitative analyses did not allow for the presence of Ba. However, visual examination of the spectrum indicated that the peak pattern more closely fit Ba. Points were analysed across the banding, and their chemical compositions indicate that it is all the same mineral, and possibly todorokite, based on the stoichiometry of that mineral. During analyses, the darker areas suffered beam damage (pits were left where the analyses were performed) while this did not occur in the brighter areas, suggesting notable variation in composition or in grain thickness. Carlos et al. (1993) reported this same experience in microprobe analyses of compositional banding in the mineral rancieite. They hypothesized that this was due to the darker bands being more hydrated than the lighter.

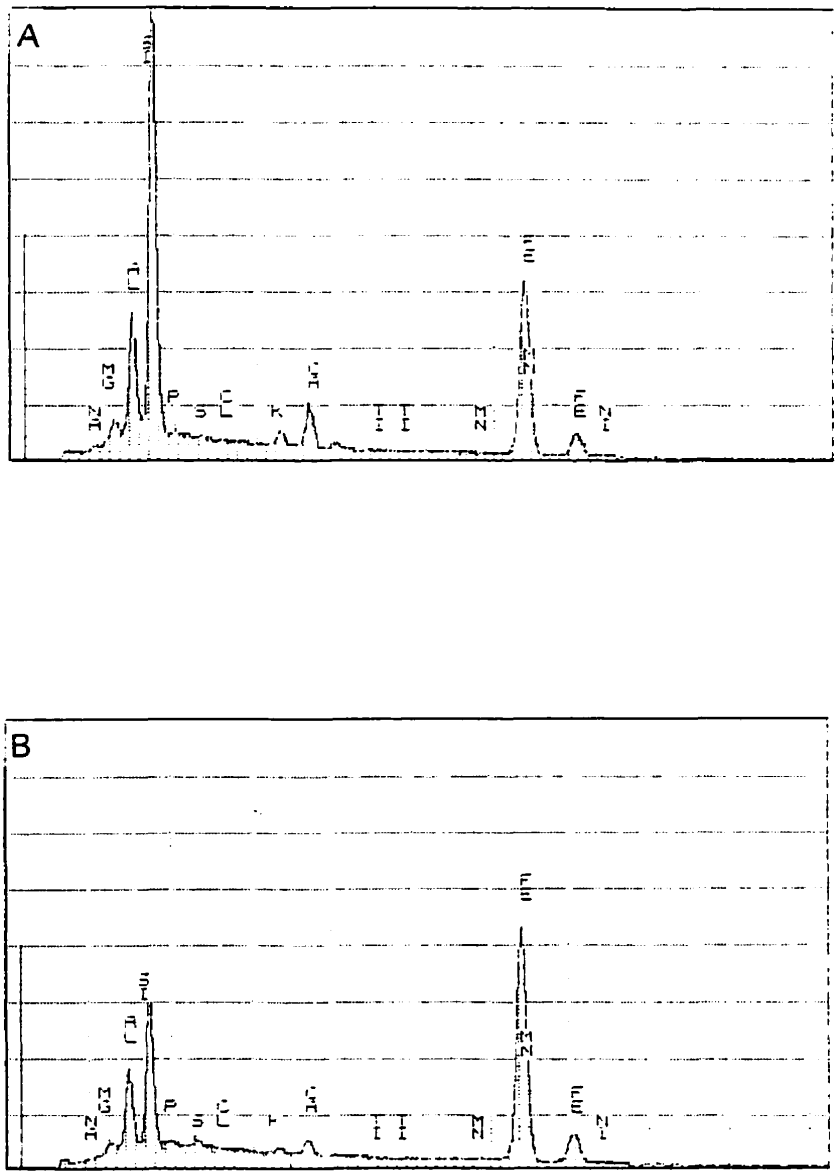

Figure 6. EDS spectra of Fe-rich coating of Laidlaw fourth horizon. A) is an analysis taken near the edge of a sample flake and B) is at the edge.
The horizontal axis indicates the energy level (0-10 eV) of detected x-ray peaks, and the vertical axis indicates relative intensity.

Table 5. Quantitative EDS analyses of banded area. Values are listed as calculated weight percents and the numbers of the first row refer to analysis number. The adjusted total reflects re-calculations based on Fe being present as Fe^{3+} instead of Fe^{2+} and Mn present as Mn^{4+}. The assumption that all Mn has an oxidation state of 4+ is not entirely accurate and represents an end-member. In reality, Mn is probably present as both Mn^{3+} and Mn^{4+}. Note: the low adjusted total is due to water present in the mineral.

	1	2	3	4	5	6	7	Avg.
SiO_2	0.6	0.8	0.9	0.8	1.1	1.0	0.9	0.9
TiO_2	0.4	0.4	0.5	0.4	0.3	0.3	0.3	0.4
Al_2O_3	1.5	3.4	3.2	3.3	3.8	4.2	3.8	3.3
Cr_2O_3	0	0	0	0.2	0	0.2	0	0.1
FeO	5.2	4.8	5.4	4.4	4.3	4.2	3.8	4.6
MnO	41.8	54.5	52.3	51.4	52.5	41.8	39.1	47.6
MgO	1.3	3.8	3.8	3.5	4.4	4.2	3.8	3.5
CaO	2.9	3.7	3.7	3.5	3.6	2.6	2.5	3.2
Na_2O	0	0.1	0	0.3	0.4	0.3	0.6	0.2
K_2O	0	0.1	0	0	0.1	0.1	0	0.0
Total	53.8	71.7	69.8	67.8	70.5	58.8	54.8	63.9
Adjusted total								74.8

3) SEM and EDS

SEM was used in conjunction with qualitative EDS to aid primarily in determining Mn-mineralogy. Because most of the Mn-oxides contain foreign cations as structural constituents, qualitative EDS can indicate what foreign cations are present, and therefore, to help narrow down the search. While a high degree of chemical variability exists with the Mn-oxides and chemical

composition is not entirely diagnostic (McKenzie, 1989), a significant concentration of the structural foreign cations would be apparent. Chemical composition has been used in conjunction with other methods, such as XRD, to identify minerals (Carlos et al., 1993). Furthermore, crystal morphology is somewhat more distinctive with the Mn-oxides than the Fe-oxides, and SEM allows for grains to be viewed at high magnification.

In addition to helping determine mineralogy, SEM also provided information on grain size and morphology of coating minerals, thus allowing evalution of surface reactivity.

Dalmeny

The Mn-minerals in the second horizon are very delicate and occur in what appear to be clusters of fibres or laths, and/or irregularly shaped platelets (Fig. 7). The grains are about 1 μm in length and orders of magnitude smaller in width. EDS analyses verify that the clusters are quite pure, with minor admixed phases, and similar composition throughout. Minor K and Ni are present as are significant quantities of Si, Fe and Ca. However, it may be that the Si and Ca peaks are from quartz and calcite under the Mn-minerals (other grains are not visible in the images) and not part of the composition of the Mn-minerals. The morphology alone suggests that the dominant mineral is vernadite, but because the chemical makeup is quite variable for the disordered mineral (Burns and Burns, 1979), the EDS analyses cannot confirm its presence.

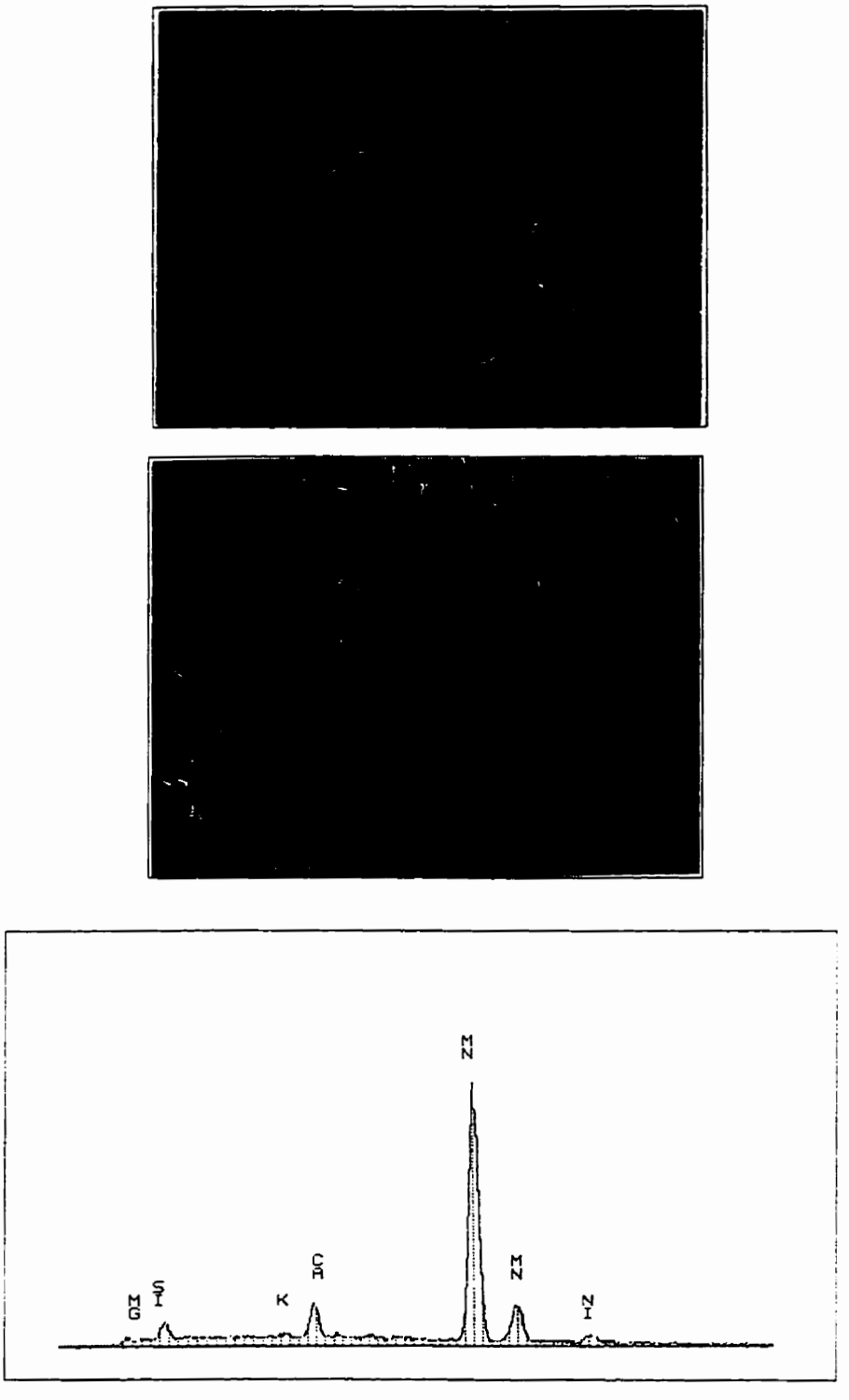

Figure7. SEM images and EDS spectrum of Dalmeny second horizon Mn-oxides. Note: second Mn peak on spectrum overlaps with main Fe peak.

Mn-oxides from the third horizon appear to be more likely laths or fibres than cross-sections of plates and also have large cloud-like masses mixed in that have the same composition (Fig. 8). The fibres are slightly longer than those in the horizon above. These nodules, while not as expansive as those from the second horizon, also appear quite uniform in composition, with minor admixed phases. There is a significant Fe peak in EDS spectra, and Ni, Ca and Si are also present again, although in lesser amounts than with the second horizon.

Examination of Fe-oxide coating areas from the third horizon that appeared, under the binocular microscope, to be quite uniform and coherent did not allow for resolution of individual Fe minerals visually or by spectroscopy. Fe-rich "desiccated crusts" were visible in some locations, but their EDS analyses yielded very high Si peaks (higher than Fe), with Ca, Al, K and Mg also present in significant proportions (Fig. 9). These results are in agreement with the petrographic and electron microprobe analyses: Fe-oxides do not exist as distinct phases as do the Mn-oxides, but are dispersed and admixed within the matrix.

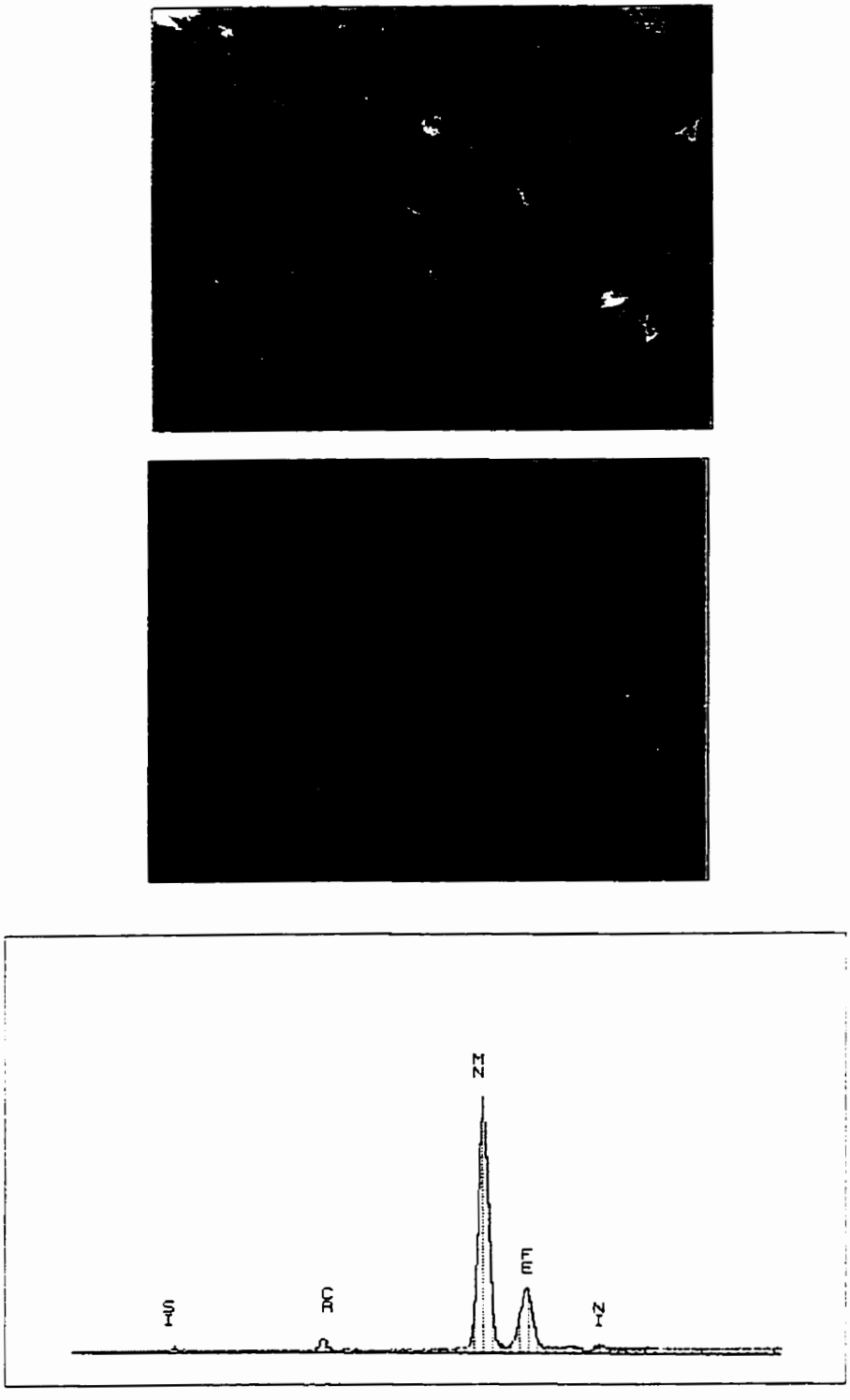

Figure 8. SEM images and EDS spectrum of Dalmeny third horizon Mn-oxides.

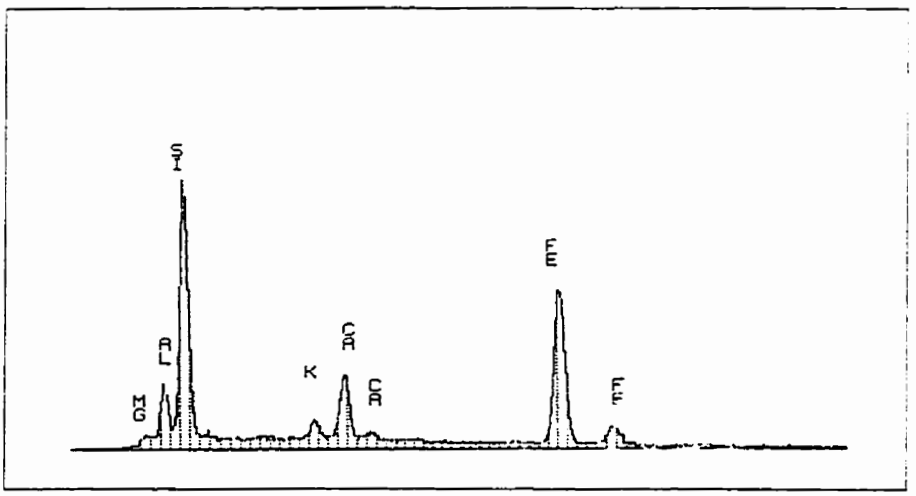

Figure 9. SEM image and EDS spectrum of Fe-rich crust from Dalmeny third horizon.

Laidlaw

A broad scan of the silvery-grey material of the second horizon yielded a spectrum typical of aluminosilicates and carbonates: large Si, Ca and Mg peaks, significant Al, lesser K, and minor Fe. The surface is extremely uniform and fine-grained suggesting that precipitation of authigenic minerals has occurred.

Mn-minerals from the third horizon are quite irregular with a "flowery" appearance. The grains are irregularly shaped platelets less than 1 μm in diameter that appear curled and folded around some of their edges (Fig. 10), such that some grains look more plate-like, while others appear to be laths. As with Dalmeny, the deposits seem fairly uniform compositionally, with minor admixed phases. The EDS spectra yield, in addition to the major Mn peak, significant Ca, Si, and Fe peaks, with lesser S, K, Al, and Ba, and occasionally, minor Ni. Again, the irregular morphology suggests vernadite, but the variation in morphology indicates that there may be more than one mineral type present. The main chemical constituents of this deposit are the same as at Dalmeny.

Mn-oxides from the fourth horizon differ significantly in appearance. The larger grains are platy, but the morphology of the smaller grains is not clear (Fig. 11). Grain size varies from approximately 1 μm to much less. With the larger grains, no Si peaks arise in EDS analyses; some Ca and Fe are present in addition to Mn, and there is also minor Al. The platy appearance of the grains suggests that the mineral is from the layered-structure group, most likely the birnessite group (Burns and Burns, 1979). The absence of Na and the high

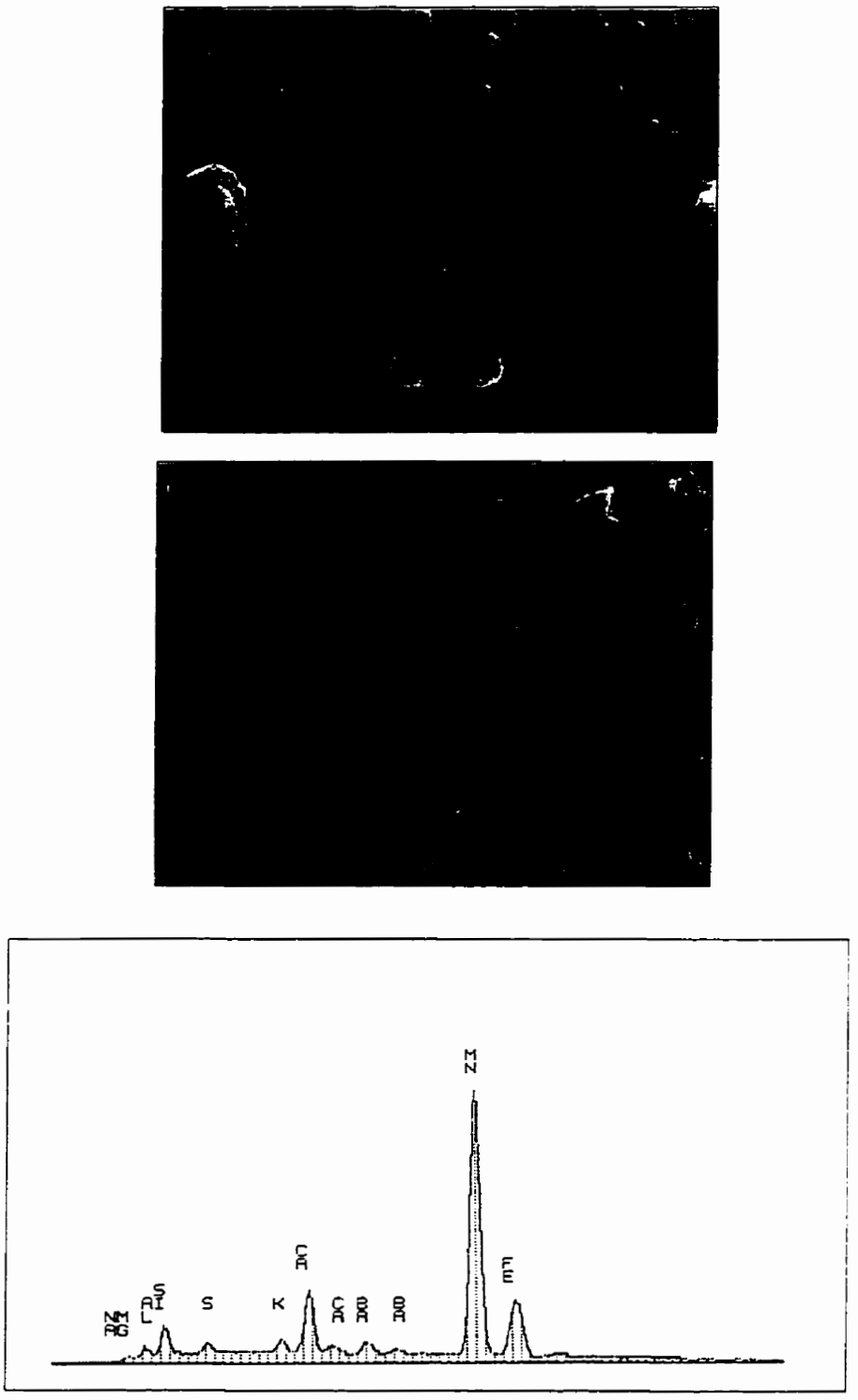

Figure 10. SEM images and EDS spectrum of Laidlaw third horizon Mn-oxides.

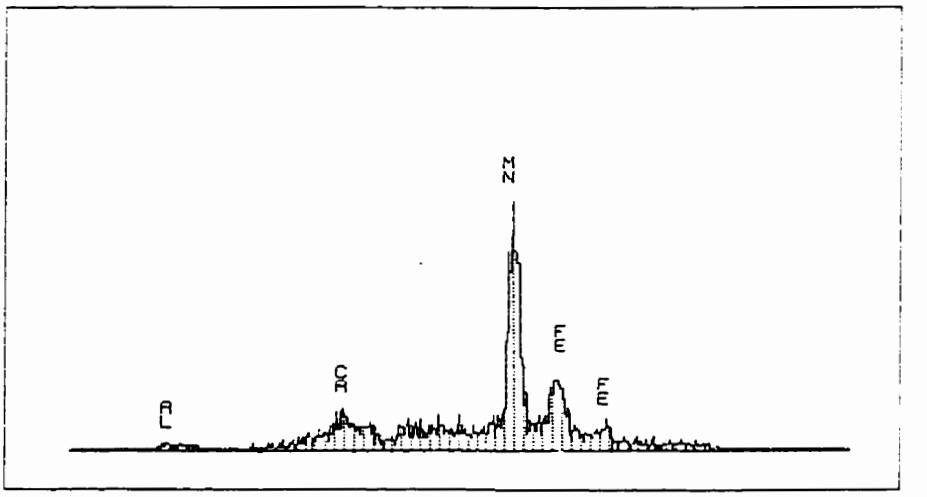

Figure 11. SEM image and EDS spectrum of Laidlaw fourth horizon Mn-oxides.

concentration of Ca suggests that the mineral is rancieite. The EDS analyses of the smaller-grained crystals (less than 1 μm) yield, in addition to Ca and Fe, significant Ba and Si peaks associated with the Mn. In some cases, there is also Al, K, and Mg, however, because detection of individual grains was more difficult due to the smaller grain size, these analyses may be also reflecting the composition of adjacent silicates.

In some heavily Fe-coated areas of the fourth horizon, the surface is flaky and regular, resembling small-scale dessication cracks. An image of a well-coated area surrounding an Mn-rich spot in this horizon shows that the Fe-deposits are generally not as uniform as the Mn-deposits (Fig. 12). Furthermore, the Mn-minerals are finer-grained. The differing uniformity of the two deposits is also illustrated by EDS analyses; in the Fe-rich areas, the Si content is approximately equal to the Fe and there also significant amounts of Mn, Al, Ca, and K, while within the Mn-deposits, only Mn occurs in significant quantity, with minor quantities of the other cations. No distinct morphology can be attributed to the Fe-oxides and it would seem that they again occur as an admixed phase amongst the matrix minerals.

Based on morphology and chemical composition, then, it appears that the Mn-oxide mineralogy may be similar in the more shallow horizons at both sites but differ at greater depths. At both sites, where present, the minerals are locally well developed and form a distinct phase of their own. The Fe-oxides are the same at both sites in that they are more dispersed, do not form isolated

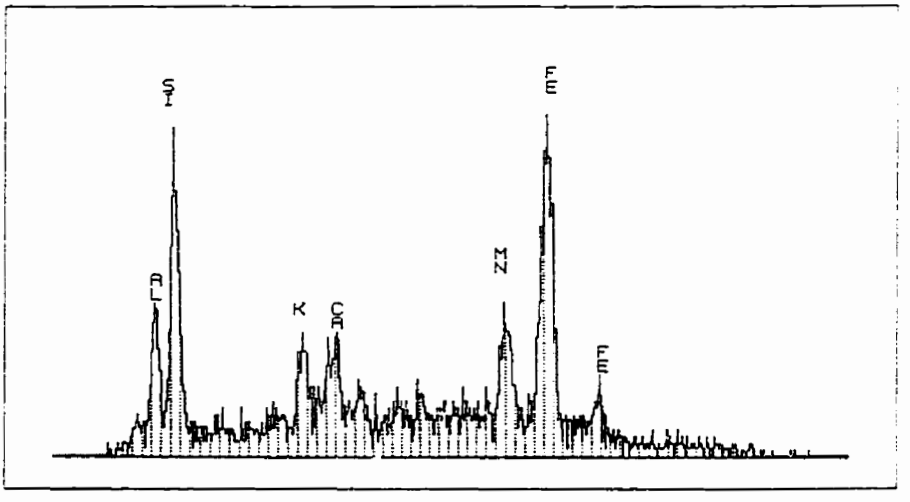

Figure 12. SEM image and EDS spectrum of Fe-rich area surrounding Mn-oxides of above image from Laidlaw fourth horizon. The Mn-oxides occur in the more uniform-looking pit in the centre.

phases in the sediments, but are forming a cement. This supports the findings of the petrographic and electron microprobe work.

4) XRD

In the early stages of this study, two quick powder XRD analyses were performed by scraping the coatings and comparing them to analyses of the matrix. Matrix mineralogy was determined to confirm the findings of previous workers (Keller et al., 1991; Quigley and Ogunbadejo, 1973).

Because the coatings are so thin, obtaining a large amount of relatively pure sample is difficult and it is not feasible to perform differential x-ray diffraction (Schulze, 1981). Because they do not require much sample, Gandolfi and Debye-Scherrer cameras were used. The samples were run for approximately 24 hours, exposed to Co radiation with an Fe filter.

Analyses using on the Debye-Scherrer camera later in the study were performed while the camera was flooded with He gas. This was found to increase the resolution of more faint lines by decreasing background noise. Background noise results from emergent x-rays being deflected by gas molecules in the sample chamber. The small atomic radius of He lessens the incidence of x-ray deflection.

In choosing samples, coatings were examined and scraped under a binocular microscope. Coating grains that looked the most uniform in composition were chosen for analyses. In reality, these were not actually grains,

but clumps of coating minerals with matrix minerals mixed in. In some cases, the samples were pre-treated with dilute hydrochloric acid to remove carbonates. However, this treatment was found to disaggregate the clumps of coating minerals making selection of sample more difficult. Matrix samples were also analysed and served as a comparison to the coating samples. Because the coatings contain so many admixed matrix phases, comparison with un-coated matrix samples was necessary for delineating coating phases. This method was used in a strictly qualitative sense, as small scale variation in matrix mineral proportions would be expected. However, even with comparison, definitive identification of coating minerals was difficult due to peak overprinting by matrix minerals, primarily quartz and illite. Furthermore, because of the small grain size and the typical poor crystallinity and cation substitution effects associated with these types of samples, XRD peaks were expected to be weak and broad, and possibly somewhat shifted; mineral identification was accomplished by looking only at the main peaks. The following criteria were used for identification of the Fe-oxides:

1) A quartz line at 0.426 nm overshadows the main goethite line at 0.418 nm. However, this line was occasionally visible as a faint line or shadow immediately following the quartz line or was suggested by an extremely broadened and intensified quartz line.

2) The second most intense goethite line, at 0.245 nm, is also overprinted, by quartz (12% I/I_o) and calcite (14%). However, the line at 0.228

nm which typically occurred 2 lines away, is also produced by both quartz and calcite at 12% quartz and 18% calcite. Comparison of the relative intensities of the 0.245 nm and the 0.228 nm lines often suggested a contribution from another mineral.

3) Finally, the 0.269-0.27 nm line, which is the third most intense line for goethite and the most intense line for hematite, was rarely overprinted. In a few instances, a very faint thin line was present which was attributed to the 10% dolomite line (dolomite was present in all samples, and identified based on its stronger lines). In most cases, though, this line was quite evident and extremely broad. In almost all samples analysed, the line occurred in addition to the above two characteristics. Goethite was identified, then, based on these three criteria.

4) Generally, the second most intense line for hematite (0.368 nm) is overprinted by illite impeding its definitive diagnosis. However, in two samples, a 0.27 nm line was clearly visible and there was definitely no goethite contribution to the quartz lines at 0.426 and 0.245 nm. In these two samples, hematite was considered to be present.

5) All ferrihydrite d-spacings are overprinted by other minerals in the samples. For both coating and matrix samples, strong broad lines occurred at 0.25-0.26 nm and 0.15 nm, corresponding to illite. A relatively strong broad line at 0.17 nm was present only in coating samples. While this value also corresponds to a d-spacing for goethite (20%), its relative intensity compared to the 0.269 nm line (35%) indicates a contribution from another mineral in all of

the samples. The other d-spacings for ferrihydrite are 0.23 and 0.197 nm, both of which are 6% quartz lines. Attempts to compare the relative intensity of these lines with other quartz lines of similar intensity were done, but proved difficult. In summary then, the relative strength of the 0.17 nm line and its presence only in coating samples, suggests the possibility of ferrihydrite being present. Definitive identification of this mineral by XRD was not, however, possible.

Dalmeny

Bulk weathered till mineralogy, taken from a sample originating at approximately 5 m depth, as determined by powder diffraction consists of quartz, clinochlore, anorthite, albite, illite, dolomite, calcite and sanidine. Samples were exposed to CrKα radiation, scanned from 18-125 degrees 2-theta for approximately 2 hours, with a step increment of 0.09

Goethite has been identified in all horizons by XRD, confirming petrographic observations.

In two samples from the taken second horizon, hematite has been recognized. The samples consisted of brighter material infilling large pores not connected with fractures. In hand specimen and under the binocular microscope, the pore infillings appeared much redder and coarser grained, and upon scraping the outermost grains, the underlying material appeared more yellow. With the first sample, which consisted of the redder surface material, the line 0.27 nm line is quite distinct and is the second most intense line on the film (after the 100% quartz line), and identifies hematite. In the second sample,

goethite is present but the relative strength of the 0.27 nm line compared to the goethite 0.418 nm indicates that hematite is also present.

The dominant, yellowish-brown coating of the second horizon proved more difficult than the other two to characterize by XRD. Lines produced by coating minerals were very minimal, and some samples analysed yielded no lines for Fe-oxide minerals. The yellow colour of the coatings suggests somewhat larger (μm-size) goethite grains (Schwertmann and Cornell, 1991) than those that might occur in other horizons. However, the difficulty of identifying any minerals other than those in the matrix from this horizon and the paleness of the colour suggest that the coating minerals are a lesser phase than in the lower horizons.

Analyses of Mn-oxides were performed but yielded no results. The minerals did not diffract x-rays, most likely because of small grain size or poor crystallinity.

XRD results indicate, then, that goethite is present in the second, third and fourth horizons, and hematite and goethite are both present in discrete pore infillings. Ferrihydrite could not be identified definitively in any horizon, nor could the Mn-oxides be distinguished.

Laidlaw

Analyses were performed on the silvery-grey material of the second horizon using the powder diffractometer in addition to Gandolfi and Debye-Scherrer cameras. A sample was run between d-spacings of approximately 2.0

and 0.5 nm (2-theta values of approximately 2 and 20, respectively) with a counting time of 15 seconds and step increment of 0.1 2-theta using CuKα radiation with a 12 μm Ni filter. This was performed in order to study potential changes in clay mineralogy evident in the higher d-spacings which would not appear on the x-ray films. Additionally, the sample was run from approximately 6 to 60 2-theta with a counting time of 6 seconds and step increment of 0.1 2-theta and compared to the matrix for any relative changes in carbonate mineralogy. Results indicate a relative increase in the proportion of carbonate minerals (especially calcite) to quartz, suggesting precipitation of carbonate minerals in this horizon. This confirms the geochemical modelling and observations of Rodvang (1987).

Goethite has been identified in the fourth horizon and the Fe-rich halo of the second horizon.

The 0.17 nm line was also present in samples from the Fe-rich horizon. It occurred as a strong, broad line, similar in intensity to the 0.269 nm line. Additionally, the strength and breadth of the 0.23 nm line compared to the other quartz lines of similar intensity in samples from this location more clearly imply a contribution from a mineral other than quartz. However, repeated illite overprinting, did not allow for resolution of the 0.25-0.26 or 0.15 nm lines, while quartz interfered with the 0.197 nm line. Consequently, ferrihydrite could not be definitely identified at this site either, although the presence of the 0.23 nm lends more support to its presence than with samples from the Dalmeny site.

XRD analyses were performed on Mn-oxide samples from the third and fourth horizons. These were compared to the results from the matrix, the Fe-rich halo in the non-oxide horizon, and analyses of the non-oxide phase, i.e. samples from adjacent areas. In all samples from the Laidlaw site, a weak to medium strength line appears at approximately 0.98 - 1.05 nm corresponding to illite. However, with all of the Mn-mineral analyses, this line was consistently stronger and broader. The line was also shifted somewhat, extending to a lower d-spacing value of approximately 0.94 nm. In one sample, taken from the third horizon, the entire line was shifted substantially lower, ranging from 0.98 to 0.88 nm. No other differences were evident in comparing the same films. While the results are far from diagnostic, the stronger line centred on average between 0.93 and 1.03 nm suggests that todorokite, whose dominant d-spacing is 0.968 nm, may be present. Alternatively, the shift in d-spacing might be a result of a compositional change in illite due to Mn-oxide formation resulting in a decreased interlayer spacing.

Chapter 7: Summary and Conclusions

The following tables summarize the analytical results for both sites:

Table 6. Summary of analytical results from the Dalmeny site. Position of water table is denoted by ▼ and depth to which a horizon occurs is indicated by ↓.

Coating horizon	Description	Petrography	SEM and EDS	XRD
Horizon 1 ↓ 3 m	Pale rusty brown Fe-oxides, calcite +/- gypsum, occasional bright spots.	**Fe-oxides**: goethite		
Horizon 2 ▼ ~4 m (leached) ↓ 5 m	Yellowish brown Fe-oxides, frequent dark brown Mn-oxide mottles, occasional bright spots.	**Fe-oxides**: goethite	**Fe-oxides**: no strong Fe peaks located. **Mn-oxides**: irregular plates & fibres, ~1µm. Composition: Significant Si, Ca and Fe. Minor K and Ni. (vernadite?)	**Fe-oxides**: goethite, hematite in bright spots. **Mn-oxides**: not detected.
Horizon 3 ▼ ~7 m (unleached) ↓ End of weathered zone (leached:8-9 m unleached: 10-12 m)	Dark rusty brown Fe-oxides, minor small black Mn-oxide spots.	**Fe-oxides**: goethite	**Fe-oxides**: Fe-rich crusts admixed with matrix. **Mn-oxides**: laths,~ >1µm Composition: Major Fe, significant Ca, minor Ni and Si.	**Fe-oxides**: goethite (+ferrihydrite?) **Mn-oxides**: not detected
Horizon 4 ↓ up to a few metres				**Fe-oxides**: goethite (+ferrihydrite?)

Table 7. Summary of analytical results from the Laidlaw site. Position of water table is denoted by ▼ and depth to which a horizon occurs is indicated by ı.

Coating Horizon	Description	Petrography and EDS	SEM and EDS	XRD
Horizon 1	Bright, slightly pinkish calcite streaks, whitish-grey non-oxide phase.			
▼ ~2 m Horizon 2	Silvery-grey material haloed by brownish-yellow Fe-oxides.		Aluminosilicates and carbonates. Fine-grained and uniform surface.	Higher proportion of carbonates. **Fe-oxides**: goethite
Horizon 3 ı End of weathered zone (~3 m)	Sooty, dark grey to black Mn-oxide mottles and dendrite with silvery-grey material as background.		**Mn-oxides**: "flowery" irregular plates, <1µm. Compositions: Significant Ca, Si and Fe, minor S, K, Al, Ba, Ni. (vernadite?)	**Mn-oxides**: not detected (todorokite?) Possible compositional change in illite
Horizon 4 ı 4-7 m	Bright rusty Fe-oxides with minor small black Mn-oxide mottles.	**Fe-oxides**: goethite **Mn-oxides**: concentric banding Composition: Major Fe, Ca, Al, Mg Minor Si, Ti (Ba?), Na, K, S, Cl (todorokite?)	**Fe-oxides**: occasional crusts, admixed with matrix. **Mn-oxides**: platy larger grains (1 µm) and unknown morphology of smaller. Compositional variation: 1) Ca, Fe, minor Al (rancieite?) 2) Ca, Fe, Ba, Si , +/- minor Al, K, Mg)	**Fe-oxides**: goethite (+ferrihydrite?) **Mn-oxides**: not detected (todorokite?)

The most significant finding regarding fracture coatings is that the Fe-oxides are not in fact "coatings" but cement. They are not a distinct phase of their own and form the interstitial material at fracture surfaces. Locally, they may form more distinct crusts overlying the matrix material. In both cases, the end result is that the formation of Fe-oxide minerals on fracture surfaces is expected to decrease the porosity of the sediments adjacent to the fracture. This decrease in porosity would translate to a locally reduced matrix permeability at fracture surfaces and would lessen the potential for diffusion of contaminants in fractures into the matrix. According to Fick's first law, the flux of a diffusing substance is the product of the effective diffusion coefficient (D*) and the solute concentration gradient. D*, which describles the diffusion of a solute through a porous medium, is the product of the tortuosity (ω) and the free solution diffusion coefficient. Tortuosity is a coefficient that accounts for the effect of the tortuous pathway through the porous medium on the ability of the solute to diffuse (Freeze and Cherry, 1979). Cementing of a porous medium would be expected to decrease the tortuosity, thereby decreasing the effective diffusion coefficient.

The impact of Fe-oxide cement at fracture surfaces on contaminant migration is independent of mineralogy. While, locally, the surface reactivity and potential for contaminant retardation may be variable over depth due to changes in Fe-oxide mineralogy, the ability of contaminants to spread laterally into the matrix will be reduced consistently.

The Fe-oxides identified are goethite, hematite and possibly ferrihydrite,

with hematite present only at the Dalmeny site. Of note is that colour was a reliable indicator of Fe-oxide mineralogy, and therefore, qualitative observations are a valuable tool.

The Mn-oxides coatings differ significantly in character from Fe-oxides. They tend to form localized, uniform deposits, perhaps in larger pores or indentations at the surface. Previous workers have found that Mn-oxides have a much greater tendency to form where other Mn-oxides already exist. The surface of an Mn-oxide grain becomes the site for autocatalytic oxidation of Mn^{2+} in solution and subsequent precipitation of further Mn-oxides (Dixon and Skinner, 1992). This explains why Mn-oxide deposits at fracture surfaces are not as extensive as the Fe-oxides.

The Mn-oxides are different between sites in terms of quantity and mineralogy. They are not as abundant at Dalmeny. The Mn-minerals could not be definitively identified at either site. However, based on morphology and chemical compositions, the dominant Mn-oxide mineralogy is similar at shallower depths at both sites and may be vernadite. At greater depths, the mineralogy differs between locations. At Laidlaw, the Mn-mineralogy of the fourth horizon is more variable than the deeper Mn-oxides at Dalmeny, and the minerals may be rancieite and todorokite.

It has been suggested by previous workers at the site (McKay, 1991; McKay and Fredericia, 1995; Klint, 1996) that the silvery-grey material of the second horizon consists of re-reduced Fe-minerals formed as a result of a rise in

the water table. The bleached look of these surfaces may be a result of Fe-oxide leaching and Fe remobilization to greater depths (Schwertmann and Taylor, 1989). Fe remobilization may be caused by more reducing conditions in recharging water, but it seems unlikely that Fe-oxides would persist at greater depths if this was the case. The material is definitely not reduced Fe-minerals because EDS analyses and XRD results have shown that there is little Fe present in this horizon. In fact, the minerals at the fracture surface consist of authigenic carbonates, and potentially authigenic aluminosilicates.

All coating minerals have a very small grain size, with the clearly visible Mn-oxides having a length (or diameter) of approximately 1 μm or less. Since they are more dispersed and intimately associated with matrix minerals, it was not possible to discern the grain size of the Fe-oxides. This small grain size translates to a potentially high surface reactivity.

Because the Fe-oxides are forming in matrix pore spaces and not actually on the fracture surface, it seems unlikely that the minerals are simply precipitating from solution within the fractures. A change in geochemical conditions is necessary to cause the Fe^{2+} in solution to be oxidized and precipitated as a ferric oxide. Within the fractures, the conditions are more oxidizing due to advective transport of oxygenated water from the surface, while in the matrix, more reducing because of slower diffusive transport and subsequent consumption of oxygen in the groundwater.

These conditions are analogous to sedimentary deposits in surface water

environments where aerated surface water is in contact with anaerobic sediments. In such environments, upward diffusion of Fe^{2+} within the sediments towards the oxygenated interface has been found to occur in response to a concentration gradient between the sediments and water column. This is what causes the accumulation of Fe-oxide layers in sedimentary deposits (Berner, 1971).

Because of the differing redox conditions between pore water of an aquitard matrix and groundwater in fractures, a gradient would also exist between the concentration of Fe^{2+} in the matrix and the concentration in fractures. Since the conditions are more reducing in the matrix, the concentration of Fe^{2+} would be greater there. This would result in diffusion of Fe^{2+} from the matrix towards the fracture. Upon nearing the fracture surface, the more oxidizing conditions would cause oxidation of Fe^{2+} to Fe^{3+} and subsequent formation of Fe-oxides. As long as groundwater moving through the fractures is more oxidizing than porewater in the matrix, this process would continue until the concentration of Fe^{2+} within the matrix was decreased to such an extent that there was no longer a significant concentration gradient between the matrix and the fracture.

At both the Dalmeny and Laidlaw sites, it is clear that secondary minerals vary with depth. This seems reasonable given that hydrogeochemical conditions should evolve with depth themselves. There will be changes in pH as groundwater moves from the soil zone into aquitard matrix, changes in solute

concentrations as some minerals precipitate while other dissolve, and, most importantly for oxide coating formation, changes in the redox state as dissolved oxygen in recharging waters is consumed.

The effect of recharging waters is most evident at the Laidlaw sites where the hydraulic significance of fractures dictates to what depth specific horizons will occur. In larger, deeper fractures, the upper horizons persist to greater depths than with smaller, less hydraulically active fractures. That we don't see this at Dalmeny may be an artifact of core sampling.

Of note at the Dalmeny site is that, despite the order of magnitude difference in hydraulic gradient between leached and unleached settings, coating horizons appear to be consistent between zones. While the horizons vary somewhat in terms of range of depth between zones, the same mineralogical changes occur, regardless of setting. This indicates that there may be more recharge occurring in the unleached settings than was previously thought.

The Fe-oxides may be used as an indicator of groundwater geochemical conditions by comparing the dominant mineralogy in the various horizons. The predominance of goethite in more shallow horizons, whose formation is favoured under conditions of slow oxidation (Schwertmann and Taylor, 1989), suggests that the geochemical gradient between the matrix and the fractures is not as great as at other depths. Where there is a significant difference between the geochemistry of the matrix and fractures, coating formation would likely be more

rapid. This would favour the precipitation of ferrihydrite (Schwertmann and Taylor). Furthermore, because hematite must form from ferrihydrite (Schwertmann and Taylor, 1989), its presence not only indicates a larger gradient, but also that the coatings at that location are relatively old. Ferrihydrite is typically considered a "young" Fe-oxide (Schwertmann and Taylor, 1989).

The formation of specific Fe-oxides at a particular depth would likely change over time, as the sedimentary unit as a whole evolves geochemically. Upon deglaciation, the geochemical gradient between fractures and matrix near surface would have been greater than at present because the matrix was not oxidized throughout, as it is presently. Ferrihydrite would probably have been the dominant Fe-oxide initially, as opposed to presently where, based on colour and XRD results, goethite dominates. One would expect that, over time, the Fe-oxide coatings forming on fractures in an unweathered matrix will be precipitating rapidly and most likely be ferrihydrite. For this reason, the Fe-oxide fracture coatings below the weathered zone would be expected to have the most reactive surfaces.

Further Work:

To develop a better understanding of local variations in geochemical conditions, more accurate mineralogical determinations are required. Transmission electron microscopy (TEM) with electron diffraction would likely be more successful in determine the mineralogy of the extremely fine-grained Mn-oxides. Infrared spectroscopy would also be useful because it is not dependent

on well-developed crystallinity, as are electron or x-ray diffraction. Furthermore, the greater resolution of TEM might allow individual grains of the Fe-oxides to be viewed and electron diffraction would likely be more successful in identifying ferrihydrite.

Actually quantifying surface reactivity using a technique like acid-oxalate extraction would be valuable. It is assumed that ferrihydrite is the Fe-oxide extracted under such treatment, and that multiplying the amount of Fe extracted by 1.7 will give the concentration of ferrihydrite in the sample (Childs, 1992). This quantity, in combination with TEM observations of typical grains size, would provide an actual measurement of surface area, and thus, potential for adsorption.

Finally, conducting experiments to determine the decrease in diffusion coefficients for various solutes and contaminant across the fracture surfaces would be extremely valuable to quantify the effect of these mineral deposits. Once quantified, this phenomenon could then be accounted for in groundwater modelling.

References:

Balfour, D. J. (1991) Evaluation of lateral solute migration in surficial weathered clayey till. M.Sc. Thesis, University of Waterloo, Waterloo, Ont.

Belzile, N. and Tessier, A. (1990) Interactions between arsenic and iron oxyhydroxides in lacustrine sediments. *Geochimica et Cosmochimica Acta* **5**, pp. 103-109.

Berner, R. A. (1969) Goethite stability and the origin of red beds. *Geochimica et Cosmochimica Acta* **33**, pp. 267-273.

Berner, R. A. (1971) *Principles of Chemical Sedimentology*. McGraw-Hill International Series in the Earth and Planetary Sciences, Montreal.

Betekhtin, A. G. (1937) New mineral species of the group of manganese hydroxides. *Zap. Vses. Mineralog. Obsheh* **66**, no. 4.

Borgaard, O. K. (1983) Effect of surface area and mineralogy of iron oxides on their surface charge and anion-adsorption properties. *Clays and Clay Minerals* **31**, pp. 230-232.

Burns, R. G. and Burns, V. M. (1979) Manganese Oxides. In *Marine Minerals* (ed R. G. Burns), Reviews in Mineralogy Vol. 6, Chap. 1, pp. 1-46. Mineralogical Society of America, Washington D.C..

Carlos, B. A., Chipera, S. J., Bish, D. L. and Craven, S. J. (1993) Fracture-lining manganese oxide minerals in silicic tuff, Yucca Mountain, Nevada, U.S.A.. *Chemical Geology* **107**, pp. 47-69.

Cerling , T. E. and Turner, R. R. (1982) Formation of freshwater Fe-Mn coatings on gravel and the behavior of ^{60}Co, ^{90}Sr, and ^{137}Cs in a small watershed. *Geochimica et Cosmochimica Acta* **46**, pp. 1333-1343.

Childs, C. W. (1992) Ferrihydrite: a review of structure, properties and ccurrence in relation to soils. *Z. Pflanzenernähr. Bodenk* **155**, pp. 441-448.

Christiansen, E. A. (1968a) A thin till in west-central Saskatchewan. *Canadian Journal of Earth Sciences* **5**, pp. 329-336.

Christiansen, E. A. (1968b) Pleistocene stratigraphy of the Saskatoon area,

Saskatchewan, Canada. *Canadian Journal of Earth Sciences* **5**, pp. 1167-1173.

Christiansen, E. A. (1979) The Wisconsinan deglaciation of southern Saskatchewan and adjacent areas. *Canadian Journal of Earth Sciences* **16**, pp. 913-938.

Chukrov, F. V., Gorshkov, A. I., Sivtsov, A. V. and Beresovskaya, V. V. (1978a) Structure varieties of todorokite. *Izvestia Akademia Nauk. SSSR. Series Geology* **12**, pp. 86-95.

Chukrov, F. V., Gorshkov, A. I., Rudnitskaya, E. S., Beresovskaya, V. V. and Sivstov, A. V. (1978b) On vernadite. *Izvestia Akademia Nauk. SSSR. Series Geology* **9**, pp. 67-76.

Chukrov, F. V., Zvyagin, B. B., Ermilova, L. P. and Gorshkov, A. I. (1973) Ferrihydrite. *Izvestia Akademia Nauk. SSSR Series Geology* **4**, pp. 23-33.

Coston, J. A., Fuller, C. C. and Davis, J. A. (1995) Pb^{2+} and Zn^{2+} adsorption by a natural aluminum- and iron-bearing surface coating on an aquifer sand. *Geochimica et Cosmochimica Acta* **59**, pp. 3535-3547.

D'Astous, A. Y., Ruland, W. W., Bruce, J. R. G., Cherry, J. A. and Gillham, R. W. (1989) Fracture effects in the shallow groundwater zone in weathered Sarnia-area clay. *Canadian Geotechnical Journal* **26**, pp. 43-56.

Desaulnier, D. E. (1986) Groundwater origin, geochemistry and solute in three major glacial clay plains of east-central North America. Ph.D. Thesis, University of Waterloo, Waterloo, Ont.

Dixon, J. B. and Skinner, H. C. W. (1992) Manganese minerals in surface environments. In *Biomineralization Processes of Iron and Manganese* (eds H. C. W. Skinner and R. W. Fitzpatrick), Catena Supplement 21, pp. 31-50. Catena Verlag, Cremlingen.

Dreimanis, A. (1964) Lake Warren and the Two Creeks Interval. *Journal of Geology* **72**, pp. 247-250.

Drever, J. I. (1988) *The Geochemistry of Natural Waters 2nd ed.* Prentice Hall, New Jersey.

Ferrier, A. (1966) L'influence de l'état de division de la goethite et l'oxyde ferrique sur leurs chaleurs de réaction. *Revue de Chimie Minérale* **3**, pp.

587-615.

Fischer, W. R. and Schwertmann, U. (1975) The formation of hematite from amorphous iron (II) hydroxide. *Clays and Clay Minerals* **23**, pp. 33-37.

Fortin, D., Leppard, G. G. and Tessier, A. (1993) Characteristics of lacustrine diagenetic iron oxyhydroxides. *Geochimica et Cosmochimica Acta* **57**, pp. 4391-4404.

Fortin, G., Van Der Kamp, G. and Cherry, J. A. (1991) Hydrogeology and hydrogeochemistry of an aquifer-aquitard system within glacial deposits, Saskatchewan, Canada. *Journal of Hydrology* **120**, pp. 203-292.

Freeze, R. A. and Cherry, J. A. (1979) *Groundwater*. Prentice-Hall, Toronto.

Goss, C. J. (1987) The kinetics and reaction mechanism of the goethite to hematite phase transformation. *Mineralogical Magazine* **51**, pp. 437-451.

Grisak, G. E. and Cherry, J. A. (1975) Hydrogeologic characteristics and response of fractured till and clay confining a shallow aquifer. *Canadian Geotechnical Journal* **12**, pp. 23-43.

Grisak, G. E., Cherry, J. A., Vonhof, J. A. and Blumele, J. P. (1976) Hydrogeologic and hydrochemical properties of fractured till in the interior plains region. In *Glacial Till* (ed R. F. Legget) Royal Society of Canada, Special Publication **12**, pp. 304-335.

Healey, T. W., Herring, A. P. and Fuerstenau, D. W. (1966) The effect of crystal structure on the surface properties of a series of manganese dioxides. *Journal of Colloid Interface Science* **21**, pp. 435-444.

Hendry, M. J., Cherry, J. A. and Wallick, E. I. (1986) Origin and distribution of sulphate in a fractured till in southern Alberta, Canada. *Water Resources Research* **22**, pp. 45-61.

Hendry, M. J. (1982) Hydraulic conductivity of a glacial till in Alberta. *Ground Water* **20**, pp. 162-169.

Jones, L. H. P. and Milne, A. A. (1956) Birnessite, a new manganese oxide mineral from Aberdeenshire, Scotland. *Mineralogical Magazine* **31**, pp. 283-288.

Jørgensen, P. R. and Fredericia, J. (1992) Migration of nutrients, pesticides and

heavy metals in fractured clayey till. *Géotechnique* **42**, pp. 67-77.

Keller C. K. Van Der Kamp, G. and Cherry, J. A. (1986) Fracture permeability and groundwater flow in clayey till near Saskatoon, Saskatchewan. *Canadian Geotechnical Journal* **23**, pp. 229-240.

Keller, C. K. and Van Der Kamp, G. (1988) Hydrogeology of two Saskatchewan tills, II. Occurrence of sulphate and implications for soil salinity. *Journal of Hydrology* **101**, pp. 123-144.

Keller, C. K., Van der Kamp, G. and Cherry, J. A. (1988) Hydrogeology of two Saskatchewan tills I. Fractures, bulk permeability, and spatial variability of downward flow. *Journal of Hydrology* **101**, pp. 97-121.

Keller, C. K., Van Der Kamp, G. and Cherry, J. A. (1991) Hydrogeochemistry of a clayey till 1. Spatial Variability. *Water Resources Research* **27**, pp. 2543-2554.

Kirkpatrick, G. (In progress) M.Sc. thesis. University of Waterloo, Waterloo, Ont.

Klint, K. E. S. (1996) Fractures and depositional features of the St. Joseph Till and upper part of the Black Shale Till at the Laidlaw site, Lambton County, Ontario. Geological Survey of Denmark and Greenland, Report 1996/9, 39 pp.

Koljonen, T., Lahermo, P. and Carlson, L. (1976) Origin, mineralogy, and chemistry of manganiferous and ferruginous precipitates found in sand and gravel deposits in Finland. *Bulletin of the Geological Society of Finland* **48**, pp. 111-135.

Langmuir, D. (1971) Particle size effect on the reaction goethite = hematite + water. *American Journal of Science* **271**, pp. 147-156.

McBride, M. B. (1994) *Environmental Chemistry of Soils.* Oxford University Press, New York.

McKay, L. D. (1991) Groundwater flow and contaminant transport in a fractured clay till. Ph.D. Thesis, University of Waterloo, Waterloo, Ont.

McKay, L. D. and Fredericia, J. (1995) Distribution, origin, and hydraulic influence of fractures in a clay-rich glacial deposit. *Canadian Geotechnical Journal* **32**, pp. 957-975.

McKay, L. D., Cherry, J. A. and Gillham, R. W. (1993a) Field experiments in a fractured clay till 1. Hydraulic conductivity and fracture aperture. *Water Resources Research* **29**, pp. 1149-1162.

McKay, L. D., Gillham, R. W. and Cherry, J. A. (1993b) Field experiments in a fractured clay till 2. Solute and colloid transport. *Water Resources Research* **29**, pp. 3879-3890.

McKenzie, R. M. (1989) Manganese Oxides and Hydroxides. In *Minerals in Soil Environments, 2nd ed* (eds J. B. Dixon and S. B. Weed) Chap 9, pp. 439-465. Soil Science Society of America. Madison.

Murray, J. W. (1979) Iron oxides. In *Marine Minerals* Reviews (ed R. G. Burns), Reviews in Mineralogy Vol. 6, Chap 2, pp. 47-98. Mineralogical Society of America, Washington D.C..

Norrish, K. and Taylor, R. M. (1961) The isomorphous replacement of iron by aluminum in soil goethites. *Journal of Soil Science* **12**, pp. 294-306.

Paterson, E. (1981) Intercalation of synthetic buserite by dodecylammonium chloride. *American Mineralogist* **66**, pp. 424-427.

Post, J. E. (1992) Crystal Structures of Manganese Oxide Minerals. In *Biomineralization Processes of Iron and Manganese* (eds H. C. W. Skinner and R. W. Fitzpatrick), Catena Supplement 21, pp. 51-74. Catena Verlag, Cremlingen.

Potter, R. M. and Rossman, G. R. (1979a) The tetravalent manganese oxides: identification, hydration, and structural relationships by infrared spectroscopy. *American Mineralogist* **64**, pp. 1199-1218.

Potter, R. M. and Rossman, G. R. (1979b) Mineralogy of manganese dendrites and coatings. *American Mineralogist* **64**, 1219-1226.

Potter, R. M. and Rossman, G. R. (1979c) The manganese- and iron-oxide mineralogy of desert varnish. *Chemical Geology* **25**, 79-94.

Quigley, R. M. and Ogunbadejo, T. A. (1973) Till geology, mineralogy and geotechnical behaviour, Sarnia, Ontario. In *Glacial Till* (ed R. F. Legget) Royal Society of Canada, Special Publication **12**, pp. 336-345.

Remenda, V. H. (1993) Origin and migration of natural groundwater tracers in thick clayey tills of Saskatchewan and the Lake Agassiz Clay Plain. Ph.D.

Thesis, University of Waterloo, Waterloo, Ont.

Richards, R. A., Sobanski, A. A. and Nunan J. P. (1984) Township of Moore waste disposal site hydrogeologic investigation. Report submitted to Tricil (Sarnia) Limited by Hydrology Consultants, Toronto, Ont.

Robinson, G. D. (1982) Trace metal adsorption potential of phases comprising black coatings on stream pebbles. *Journal of Geochemical Exploration* **17**, pp. 205-219.

Rodvang, S. J. (1987) Geochemistry of the weathered zone of a fractured clayey deposit in southwestern Ontario. M.Sc. Thesis, University of Waterloo, Waterloo, Ont.

Ruland, W. W., Cherry, J. A. and Feenstra, S. (1991) The depth of fractures and active ground-water flow in a clayey till plain in southwestern Ontario. *Ground Water* **29**, pp. 405-417.

Schulze, D. G. (1981) Identification of soil iron oxide minerals by differential x-ray diffraction. *Soil Science Society of America Journal* **45**, pp. 437-440.

Schwertmann U., Schulze, D. G. and Murad, E. (1982) Identification of ferrihydrite in soils by dissolution kinetics, differential x-ray diffraction and Mössbauer spectroscopy. *Soil Science Society of America Journal* **46**, pp. 869-875.

Schwertmann, U. and Fechter H. (1982) The point of zero charge of natural and synthetic ferrihydrites and its relation to absorbed silicate. *Clay Minerals* **17**, pp. 471-476.

Schwertmann, U., Fitzpatrick, R. W., Taylor, R. M. and Lewis, D. G. (1979) The influence of aluminum on iron oxides. Part II. Preparation and properties of Al substituted hematites. *Clays and Clay Minerals* **27**, pp. 105-112.

Schwertmann, U. and Taylor, R. M. (1989) Iron oxides. In *Minerals in Soil Environments, 2nd ed* (eds. J. B. Dixon and S. B. Weed) Chap 8, pp. 379-438. Soil Science Society of America. Madison.

Schwertmann, U. and Cornell, R. M. (1991) *Iron Oxides in the Laboratory*. VCH Publishers Inc., New York.

Stiers, W. and Schwertmann, U. (1985) Evidence for manganese substitution in synthetic goethite. *Geochimica et Cosmochimica Acta* **49**, pp. 1909-1911.

Taylor, R. M. and Schwertmann, U. (1978) The influence of aluminum on iron oxides. Part I. The influence of Al on Fe oxide formation from the Fe(II) system. *Clays and Clay Minerals* **26**, 373-383.

Taylor, R. M. and Schwertmann, U. (1974) Maghemite is soils and its origin. II. Maghemite syntheses at ambient temperature and pH 7. *Clay Minerals* **10**, pp. 299-310.

Zwicker, W.K., Meijer, W. O. J. G. and Jaffe, H. W. (1962) Nsutite - a widespread manganese oxide mineral. *American Mineralogist* **47**, pp. 246-266.

Appendix A

XRD Data

Tables are spreadsheets used to calculate d-spacings based on line-positions on films and radiation wavelength according to Bragg's Law.

Legend:
LHS: Position of line at left-hand side of film center point.
RHS: Position of line at right-hand side of film center point.
4O, 20 and 0: 4-theta, 2-theta and theta values calculated from line position on film and radiation wavelength according to Bragg's law.
d-sp: d-spacings.
center: indicates center position of film. Consistency in center point position is a measure of accurate location of lines.
w, v.w., med., str., br.: descriptions of lines, referring to weak, very weak, medium, strong, and broad, respectively.
"2 edges of" marks the beginning of a two-line intensity comment and indicates the d-spacing value refers to the edge of a broad line with the following d-spacing the other edge of the line.

Table A.1. Dalmeny second horizon Fe-oxides. Note: d-spacing values in all the tables are listed in angstroms.

LHS	RHS	4O	2O	O	d-sp	center	Intensity
77.05	97.50	20.45	10.23	5.11	10.05	87.28	
75.10	99.70	24.60	12.30	6.15	8.36	87.40	v.w
68.10	97.05	28.95	14.48	7.24	7.11	82.57	
61.70	103.05	41.35	20.67	10.34	4.99	82.38	w.br
59.25	105.50	46.25	23.12	11.56	4.47	82.38	
62.80	112.05	49.25	24.62	12.31	4.20	87.42	2 edges of
63.50	111.50	48.00	24.00	12.00	4.31	87.50	quartz line
61.75	113.25	51.50	25.75	12.88	4.02	87.50	
60.00	115.35	55.35	27.67	13.84	3.74	87.68	v.v.w
59.00	115.85	56.85	28.42	14.21	3.65	87.42	v.v.w
57.30	117.15	59.85	29.93	14.96	3.47	87.22	v.w
56.35	118.60	62.25	31.12	15.56	3.34	87.48	
55.40	119.90	64.50	32.25	16.12	3.22	87.65	2 edges of
54.55	120.45	65.90	32.95	16.48	3.16	87.50	broad line
52.55	122.40	69.85	34.93	17.46	2.98	87.48	2 fuzzy, weak
51.65	123.30	71.65	35.83	17.91	2.91	87.48	close lines
49.50	125.35	75.85	37.92	18.96	2.75	87.42	v.w
47.30	127.80	80.50	40.25	20.12	2.60	87.55	2 edges of
46.00	128.95	82.95	41.47	20.74	2.53	87.48	strong broad line
14.20	160.70	146.50	73.25	36.62	1.50	87.45	

Table A.2. Bright spot with hematite from Dalmeny second horizon.

LHS	RHS	4O	2O	O	d-sp	center	Intensity
52.60	100.80	48.20	24.10	12.05	4.29	76.70	
46.95	107.60	60.65	30.32	15.16	3.42	77.28	100
43.85	109.65	65.80	32.90	16.45	3.16	76.75	
38.40	115.15	76.75	38.38	19.19	2.72	76.78	2nd
33.60	119.90	86.30	43.15	21.58	2.43	76.75	4th
29.30	124.25	94.95	47.48	23.74	2.22	76.78	
21.35	132.30	110.95	55.48	27.74	1.92	76.83	
18.95	135.50	116.55	58.28	29.14	1.84	77.22	
10.50	142.90	132.40	66.20	33.10	1.64	76.70	3rd
7.25	146.25	139.00	69.50	34.75	1.57	76.75	
6.00	147.60	141.60	70.80	35.40	1.55	76.80	
3.80	149.70	145.90	72.95	36.47	1.51	76.75	
0.85	152.65	151.80	75.90	37.95	1.46	76.75	
-4.40	157.90	162.30	81.15	40.58	1.38	76.75	
30.90	122.80	91.90	45.95	22.98	2.29	76.85	

Table A.3. Dalmeny third horizon Fe-oxides.

LHS	RHS	4O	2O	O	d-sp	center	Intensity
62.30	108.50	46.20	23.10	11.55	4.47	85.40	w
61.20	109.55	48.35	24.17	12.09	**4.27**	85.38	two edges of
60.65	110.15	49.50	24.75	12.38	4.18	85.40	line
59.70	111.20	51.50	25.75	12.88	4.02	85.45	v.w.
54.30	116.45	62.15	31.08	15.54	**3.34**	85.38	100%
52.95	118.75	65.80	32.90	16.45	3.16	85.85	w.br.
51.00	119.60	68.60	34.30	17.15	3.04	85.30	w.
49.40	121.55	72.15	36.08	18.04	2.89	85.48	
46.35	124.40	78.05	39.03	19.51	2.68	85.38	VERY br.w.
44.30	126.75	82.45	41.22	20.61	2.54	85.52	br.
42.45	128.00	85.55	42.78	21.39	**2.45**	85.22	br. fairly strong
39.20	131.55	92.35	46.18	23.09	**2.28**	85.38	
38.25	132.50	94.25	47.12	23.56	**2.24**	85.38	
37.25	133.40	96.15	48.08	24.04	2.20	85.32	
35.55	135.10	99.55	49.78	24.89	**2.13**	85.32	
32.65	138.00	105.35	52.68	26.34	2.02	85.32	
31.45	139.25	107.80	53.90	26.95	**1.98**	85.35	
29.40	141.30	111.90	55.95	27.98	1.91	85.35	VERY w.
26.30	144.25	117.95	58.98	29.49	**1.82**	85.28	
25.05	145.45	120.40	60.20	30.10	1.78	85.25	br.
20.55	150.15	129.60	64.80	32.40	**1.67**	85.35	v.br.
14.35	156.25	141.90	70.95	35.48	**1.54**	85.30	
12.00	158.85	146.85	73.42	36.71	1.50	85.42	br.
9.30	161.35	152.05	76.02	38.01	**1.45**	85.32	br.
4.75	165.95	161.20	80.60	40.30	**1.38**	85.35	
3.95	166.70	162.75	81.38	40.69	**1.37**	85.32	

Table A.5. Dalmeny fourth horizon Fe-oxides.

LHS	RHS	4O	2O	O	d-sp	center	Intensity
77.40	97.25	19.85	9.92	4.96	10.35	87.32	vw
73.10	101.80	28.70	14.35	7.18	7.17	87.45	vvw
66.50	107.80	41.30	20.65	10.32	4.99	87.15	w.br
64.30	110.10	45.80	22.90	11.45	4.51	87.20	w.br
63.10	111.40	48.30	24.15	12.08	4.28	87.25	med
62.55	111.85	49.30	24.65	12.32	4.19	87.20	
58.90	115.35	56.45	28.22	14.11	3.67	87.12	vw
57.30	117.00	59.70	29.85	14.92	3.48	87.15	vw
60.50	113.95	53.45	26.72	13.36	3.87	87.22	vw
56.10	118.38	62.28	31.14	15.57	3.33	87.24	100%
54.60	119.80	65.20	32.60	16.30	3.19	87.20	med-w
52.65	121.55	68.90	34.45	17.23	3.02	87.10	med-w
50.90	123.50	72.60	36.30	18.15	2.87	87.20	med-str
49.85	124.55	74.70	37.35	18.67	2.80	87.20	vw
48.05	126.30	78.25	39.12	19.56	2.67	87.18	med-w br
46.45	127.90	81.45	40.72	20.36	2.57	87.18	med-w br
44.35	130.00	85.65	42.82	21.41	2.45	87.18	med br
43.05	131.20	88.15	44.08	22.04	2.39	87.12	vvw
40.85	133.35	92.50	46.25	23.12	2.28	87.10	w br
40.00	134.40	94.40	47.20	23.60	2.24	87.20	w br
38.85	135.50	96.65	48.32	24.16	2.19	87.18	med-w
37.60	136.70	99.10	49.55	24.78	2.14	87.15	w
36.00	138.35	102.35	51.18	25.59	2.07	87.18	vvw
34.40	139.85	105.45	52.72	26.36	2.02	87.12	w
33.35	141.00	107.65	53.82	26.91	1.98	87.18	w
31.22	143.00	111.78	55.89	27.94	1.91	87.11	vw
29.90	144.45	114.55	57.27	28.64	1.87	87.17	vw
28.05	146.50	118.45	59.22	29.61	1.81	87.28	med

26.90	147.40	120.50	60.25	30.12	1.78	87.15	med
24.30	150.10	125.80	62.90	31.45	1.72	87.20	med-w v.br
22.40	152.10	129.70	64.85	32.42	1.67	87.25	med-w br
17.70	156.50	138.80	69.40	34.70	1.57	87.10	vw br
16.15	158.20	142.05	71.02	35.51	1.54	87.17	med
14.35	160.00	145.65	72.82	36.41	1.51	87.18	vw br
10.95	163.10	152.15	76.08	38.04	1.45	87.02	vw br
8.20	166.00	157.80	78.90	39.45	1.41	87.10	vw br
6.45	168.10	161.65	80.82	40.41	1.38	87.28	med
5.75	168.75	163.00	81.50	40.75	1.37	87.25	med

Table A.5. Dalmeny matrix.

LHS	RHS	4O	2O	O	d-sp	center	Intensity
79.65	100.20	20.55	10.27	5.14	10.00	89.93	
77.70	102.15	24.45	12.23	6.11	8.41	89.93	w.
75.50	104.40	28.90	14.45	7.23	7.12	89.95	s.br.
73.90	105.90	32.00	16.00	8.00	6.43	89.90	
72.45	107.45	35.00	17.50	8.75	5.88	89.95	
69.20	110.80	41.60	20.80	10.40	4.96	90.00	br.
66.85	113.15	46.30	23.15	11.58	4.46	90.00	
65.55	114.30	48.75	24.38	12.19	4.24	89.92	
64.25	115.75	51.50	25.75	12.88	4.02	90.00	
63.15	116.75	53.60	26.80	13.40	3.86	89.95	
61.85	117.80	55.95	27.98	13.99	3.70	89.82	
61.45	118.25	56.80	28.40	14.20	3.65	89.85	
60.00	119.80	59.80	29.90	14.95	3.47	89.90	
58.90	121.00	62.10	31.05	15.52	3.34	89.95	
57.65	122.40	64.75	32.38	16.19	3.21	90.02	
56.65	123.15	66.50	33.25	16.62	3.13	89.90	w.
55.60	124.20	68.60	34.30	17.15	3.04	89.90	
54.50	125.15	70.65	35.33	17.66	2.95	89.82	v.w
53.80	126.05	72.25	36.12	18.06	2.89	89.92	
51.95	127.70	75.75	37.88	18.94	2.76	89.82	v.w.
50.65	129.15	78.50	39.25	19.62	2.67	89.90	v.w.
49.80	129.95	80.15	40.07	20.04	2.61	89.88	2 edges of
48.55	131.35	82.80	41.40	20.70	2.53	89.95	br str line
47.75	132.10	84.35	42.18	21.09	2.49	89.92	v.w.
47.15	132.65	85.50	42.75	21.38	2.46	89.90	
46.15	133.70	87.55	43.77	21.89	2.40	89.92	
44.75	135.00	90.25	45.12	22.56	2.33	89.88	w.
43.70	136.10	92.40	46.20	23.10	2.28	89.90	
42.75	137.15	94.40	47.20	23.60	2.24	89.95	
41.70	138.15	96.45	48.22	24.11	2.19	89.93	
40.90	139.00	98.10	49.05	24.52	2.16	89.95	v.w.
40.15	139.65	99.50	49.75	24.88	2.13	89.90	
39.20	140.60	101.40	50.70	25.35	2.09	89.90	w.
38.45	141.40	102.95	51.48	25.74	2.06	89.93	w
37.15	142.65	105.50	52.75	26.38	2.01	89.90	
36.20	143.75	107.55	53.78	26.89	1.98	89.98	

33.95	145.80	111.85	55.92	27.96	1.91	89.88	br
32.80	147.00	114.20	57.10	28.55	1.87	89.90	
31.95	147.90	115.95	57.98	28.99	1.85	89.92	
30.90	148.90	118.00	59.00	29.50	1.82	89.90	3 all
30.30	149.45	119.15	59.58	29.79	1.80	89.88	close
29.75	150.15	120.40	60.20	30.10	1.78	89.95	together
27.60	151.80	124.20	62.10	31.05	1.74	89.70	v.v.w.br
24.90	154.85	129.95	64.97	32.49	1.67	89.88	
22.95	157.00	134.05	67.03	33.51	1.62	89.98	v.w
22.05	157.90	135.85	67.92	33.96	1.60	89.98	
20.20	159.60	139.40	69.70	34.85	1.57	89.90	
18.95	160.95	142.00	71.00	35.50	1.54	89.95	
17.95	161.95	144.00	72.00	36.00	1.52	89.95	v.w
17.25	162.75	145.50	72.75	36.38	1.51	90.00	2 edges of
16.00	164.10	148.10	74.05	37.02	1.49	90.05	br str line
14.65	165.25	150.60	75.30	37.65	1.47	89.95	
13.85	166.10	152.25	76.12	38.06	1.45	89.98	
13.20	166.75	153.55	76.78	38.39	1.44	89.98	v.w
12.30	167.55	155.25	77.62	38.81	1.43	89.92	v.w
11.25	168.35	157.10	78.55	39.28	1.41	89.80	v.v.w
10.75	169.20	158.45	79.22	39.61	1.40	89.98	v.v.w
9.40	170.60	161.20	80.60	40.30	1.38	90.00	
8.60	171.30	162.70	81.35	40.68	1.37	89.95	
7.00	172.80	165.80	82.90	41.45	1.35	89.90	v.w
5.80	174.20	168.40	84.20	42.10	1.34	90.00	v.w

Table A.6. Silver material of Laidlaw second horizon.

LHS	RHS	4O	2O	O	d-sp	center	Intensity
102.90	118.10	15.20	7.60	3.80	13.51	110.50	
100.75	121.30	20.55	10.27	5.14	10.00	111.02	
96.20	125.50	29.30	14.65	7.32	7.02	110.85	
91.15	131.60	40.45	20.22	10.11	5.10	111.38	v.v.w
88.85	134.10	45.25	22.62	11.31	4.56	111.48	
86.70	135.25	48.55	24.28	12.14	4.26	110.98	w
85.45	136.65	51.20	25.60	12.80	4.04	111.05	w
84.10	137.75	53.65	26.83	13.41	3.86	110.92	w
82.95	138.85	55.90	27.95	13.97	3.71	110.90	w
81.70	140.45	58.75	29.37	14.69	3.53	111.07	w
81.00	141.95	60.95	30.47	15.24	3.41	111.48	100%
78.70	143.40	64.70	32.35	16.18	3.21	111.05	br. w.
76.70	145.30	68.60	34.30	17.15	3.04	111.00	
74.90	148.00	73.10	36.55	18.27	2.85	111.45	
71.65	151.00	79.35	39.67	19.84	2.64	111.32	v.br. 2
69.90	152.00	82.10	41.05	20.52	2.55	110.95	edges
68.95	152.90	83.95	41.98	20.99	2.50	110.93	v.w.
68.25	153.60	85.35	42.68	21.34	2.46	110.92	
67.40	154.70	87.30	43.65	21.82	2.41	111.05	
64.80	157.20	92.40	46.20	23.10	2.28	111.00	
64.00	158.05	94.05	47.03	23.51	2.24	111.02	
62.90	159.05	96.15	48.08	24.04	2.20	110.98	
61.25	160.75	99.50	49.75	24.88	2.13	111.00	
60.30	161.65	101.35	50.68	25.34	2.09	110.98	
59.95	162.75	102.80	51.40	25.70	2.06	111.35	v.w.
58.25	163.60	105.35	52.68	26.34	2.02	110.92	
57.40	164.60	107.20	53.60	26.80	1.99	111.00	
55.05	166.85	111.80	55.90	27.95	1.91	110.95	
53.85	168.05	114.20	57.10	28.55	1.87	110.95	
53.00	168.90	115.90	57.95	28.98	1.85	110.95	v.w
52.20	169.95	117.75	58.87	29.44	1.82	111.07	
50.95	171.15	120.20	60.10	30.05	1.79	111.05	
46.30	176.65	130.35	65.18	32.59	1.66	111.48	
43.45	178.80	135.35	67.68	33.84	1.61	111.13	v.w.
41.65	180.60	138.95	69.47	34.74	1.57	111.12	v.w.
40.25	181.85	141.60	70.80	35.40	1.55	111.05	

38.10	184.00	145.90	72.95	36.48	1.51	111.05	
35.95	186.25	150.30	75.15	37.58	1.47	111.10	
31.05	190.90	159.85	79.92	39.96	1.39	110.98	2 edges of
30.50	191.70	161.20	80.60	40.30	1.38	111.10	broad line
29.85	192.20	162.35	81.18	40.59	1.38	111.02	

Table A.7. Summary of high d-spacing variation with Dalmeny Mn-oxides.

LMnhor-1							
49.25	97.90	48.65	24.33	12.16	4.25	73.58	quartz
42.50	104.65	62.15	31.08	15.54	3.34	73.58	quartz
39.25	107.95	68.70	34.35	17.18	3.03	73.60	calc
63.10	84.15	21.05	10.53	5.26	9.76	73.62	2 edges of strong
61.90	85.25	23.35	11.68	5.84	8.80	73.58	broad line
LMnFehor-1							
55.25	117.40	62.15	31.08	15.54	3.34	86.32	
52.00	120.70	68.70	34.35	17.18	3.03	86.35	
38.15	134.65	96.50	48.25	24.12	2.19	86.40	
76.35	96.35	20.00	10.00	5.00	10.27	86.35	2 edges of med
75.50	97.20	21.70	10.85	5.43	9.47	86.35	broad line
MnLi3C-1							
52.15	100.80	48.65	24.32	12.16	4.25	76.47	quartz
45.40	107.50	62.10	31.05	15.52	3.34	76.45	quartz
40.25	112.60	72.35	36.17	18.09	2.88	76.42	dol
66.35	86.60	20.25	10.12	5.06	10.14	76.47	2 edges of strong
65.60	87.35	21.75	10.88	5.44	9.45	76.47	broad line
MnLiDa3C-2							
59.10	107.75	48.65	24.32	12.16	4.25	83.42	quartz
52.35	114.50	62.15	31.08	15.54	3.34	83.42	quartz
47.20	119.60	72.40	36.20	18.10	2.88	83.40	dol
73.35	93.50	20.15	10.08	5.04	10.19	83.42	2 edges of strong
72.50	94.50	22.00	11.00	5.50	9.34	83.50	broad line
MGS3I-1							
63.80	112.45	48.65	24.33	12.16	4.25	88.12	quartz
57.15	119.20	62.05	31.02	15.51	3.35	88.18	quartz
52.00	124.25	72.25	36.12	18.06	2.89	88.12	dol
78.35	97.90	19.55	9.78	4.89	10.51	88.12	2 edges of med
77.65	98.60	20.95	10.47	5.24	9.81	88.12	semi-broad line
MGS3I-2							
61.00	109.75	48.75	24.38	12.19	4.24	85.38	quartz
54.25	116.50	62.25	31.12	15.56	3.34	85.38	quartz
49.20	121.50	72.30	36.15	18.08	2.89	85.35	dol
75.35	95.40	20.05	10.03	5.01	10.24	85.38	2 edges of med
74.85	95.90	21.05	10.53	5.26	9.76	85.38	line

Matrix							
55.35	104.05	48.70	24.35	12.18	4.24	79.70	quartz
48.65	110.80	62.15	31.08	15.54	3.34	79.72	quartz
36.95	122.55	85.60	42.80	21.40	2.45	79.75	quartz
69.25	90.20	20.95	10.48	5.24	9.81	79.72	distinct med line
LFeHalo-1							
47.90	110.05	62.15	31.08	15.54	3.34	78.97	quartz
44.55	113.40	68.85	34.43	17.21	3.02	78.97	calc
42.75	115.10	72.35	36.17	18.09	2.88	78.92	dol
68.95	88.95	20.00	10.00	5.00	10.27	78.95	2 edges of med
68.50	89.40	20.90	10.45	5.23	9.83	78.95	semi-broad line

Table A.8. Fe-rich halo of Laidlaw second horizon.

LHS	RHS	4O	2O	O	d-sp	center	Intensity
72.40	92.95	20.55	10.27	5.14	10.00	82.68	med-str
67.90	97.45	29.55	14.77	7.39	6.96	82.68	med-w
65.50	100.00	34.50	17.25	8.62	5.97	82.75	v.w
61.95	103.50	41.55	20.78	10.39	4.96	82.72	med-w
59.60	105.75	46.15	23.08	11.54	4.48	82.68	med
58.35	107.00	48.65	24.32	12.16	4.25	82.68	med-str
57.70	107.65	49.95	24.98	12.49	4.14	82.68	w
57.10	108.55	51.45	25.72	12.86	4.02	82.82	w
55.90	109.60	53.70	26.85	13.42	3.86	82.75	w
54.40	111.00	56.60	28.30	14.15	3.66	82.70	w.br
53.15	112.30	59.15	29.58	14.79	3.51	82.72	w.br
51.60	113.85	62.25	31.12	15.56	3.34	82.72	100%
50.15	115.10	64.95	32.47	16.24	3.20	82.62	med-w, br
48.25	117.15	68.90	34.45	17.23	3.02	82.70	str
46.50	118.90	72.40	36.20	18.10	2.88	82.70	str
45.00	120.25	75.25	37.62	18.81	2.78	82.62	v.vw
43.45	122.10	78.65	39.32	19.66	2.66	82.78	med-w
42.35	123.10	80.75	40.38	20.19	2.59	82.72	2 edges of br
41.40	124.10	82.70	41.35	20.67	2.54	82.75	med line
40.60	124.85	84.25	42.12	21.06	2.49	82.72	vw
39.80	125.65	85.85	42.92	21.46	2.45	82.72	med
38.85	126.70	87.85	43.92	21.96	2.39	82.78	med-w, br
36.45	128.90	92.45	46.22	23.11	2.28	82.68	med
35.50	129.80	94.30	47.15	23.58	2.24	82.65	w
34.40	131.05	96.65	48.32	24.16	2.19	82.72	med
33.50	131.80	98.30	49.15	24.58	2.15	82.65	vvw
32.70	132.60	99.90	49.95	24.98	2.12	82.65	w
32.00	133.50	101.50	50.75	25.38	2.09	82.75	w
31.10	134.35	103.25	51.62	25.81	2.06	82.72	vvw
29.85	135.55	105.70	52.85	26.43	2.01	82.70	med
28.85	136.65	107.80	53.90	26.95	1.98	82.75	w
26.80	138.70	111.90	55.95	27.98	1.91	82.75	med
25.50	139.85	114.35	57.18	28.59	1.87	82.68	med
24.65	140.65	116.00	58.00	29.00	1.85	82.65	vw
23.50	141.85	118.35	59.18	29.59	1.81	82.68	3 lines
23.05	142.20	119.15	59.58	29.79	1.80	82.62	all close

22.40	143.00	120.60	60.30	30.15	1.78	82.70	together
19.70	145.70	126.00	63.00	31.50	1.71	82.70	w.br
17.90	147.55	129.65	64.82	32.41	1.67	82.72	w.br
15.85	149.65	133.80	66.90	33.45	1.62	82.75	vw
14.90	150.70	135.80	67.90	33.95	1.60	82.80	w
12.90	152.50	139.60	69.80	34.90	1.56	82.70	vvw
11.70	153.85	142.15	71.08	35.54	1.54	82.78	med-str
10.65	154.95	144.30	72.15	36.07	1.52	82.80	vw
9.60	155.95	146.35	73.18	36.59	1.50	82.78	med-w, br
7.40	158.15	150.75	75.38	37.69	1.46	82.78	w
2.05	163.20	161.15	80.57	40.29	1.38	82.62	w,br
1.30	164.20	162.90	81.45	40.72	1.37	82.75	med

Table A.9. Fe-oxides of Laidlaw fourth horizon.

LHS	RHS	4O	2O	O	d-sp	center	Intensity
77.40	90.90	13.50	6.75	3.38	15.20	84.15	med. v.br
74.20	94.80	20.60	10.30	5.15	9.97	84.50	br.
70.40	99.10	28.70	14.35	7.17	7.17	84.75	w
63.50	105.85	42.35	21.17	10.59	4.87	84.68	2 edges of
64.55	104.50	39.95	19.98	9.99	5.16	84.52	med br line
62.10	107.45	45.35	22.68	11.34	4.55	84.78	2 edges
61.30	108.10	46.80	23.40	11.70	4.41	84.70	of med. br. line
60.75	108.70	47.95	23.98	11.99	4.31	84.72	2 edges of
59.60	109.90	50.30	25.15	12.58	4.11	84.75	str. br. line
58.10	110.45	52.35	26.18	13.09	3.95	84.28	v.w blurry
56.55	112.95	56.40	28.20	14.10	3.67	84.75	w
55.05	114.50	59.45	29.72	14.86	3.49	84.78	w
53.80	115.85	62.05	31.02	15.51	3.35	84.82	br.100%
52.40	117.35	64.95	32.47	16.24	3.20	84.88	w
50.65	119.15	68.50	34.25	17.12	3.04	84.90	med
48.75	120.90	72.15	36.08	18.04	2.89	84.82	str.
46.50	123.40	76.90	38.45	19.23	2.72	84.95	2edges of
45.65	124.10	78.45	39.22	19.61	2.67	84.88	med line
44.65	124.95	80.30	40.15	20.08	2.61	84.80	2 edges of
43.85	125.90	82.05	41.03	20.51	2.55	84.88	med line
42.80	127.05	84.25	42.12	21.06	2.49	84.92	2 edges of str, br. line
41.40	128.60	87.20	43.60	21.80	2.41	85.00	with diffuse edges
39.05	130.80	91.75	45.88	22.94	2.30	84.93	1 broad line or
37.90	131.95	94.05	47.02	23.51	2.24	84.92	2 close lines
36.90	133.00	96.10	48.05	24.02	2.20	84.95	med-str
35.30	134.50	99.20	49.60	24.80	2.13	84.90	w
34.30	135.65	101.35	50.68	25.34	2.09	84.98	vw
32.70	136.40	103.70	51.85	25.92	2.05	84.55	med, somewhat br.
31.50	138.70	107.20	53.60	26.80	1.99	85.10	w
29.55	140.25	110.70	55.35	27.68	1.93	84.90	med to w, ~br
28.00	141.85	113.85	56.92	28.46	1.88	84.92	
26.40	143.80	117.40	58.70	29.35	1.83	85.10	2 med-str lines
25.10	144.90	119.80	59.90	29.95	1.79	85.00	close together (3?)
22.50	147.35	124.85	62.42	31.21	1.73	84.92	med-str. br line
20.60	149.50	128.90	64.45	32.22	1.68	85.05	w.br

17.65	152.65	135.00	67.50	33.75	1.61	85.15	w
15.85	154.40	138.55	69.28	34.64	1.57	85.12	w
14.55	155.70	141.15	70.57	35.29	1.55	85.12	med-str
12.50	157.90	145.40	72.70	36.35	1.51	85.20	med
10.25	160.35	150.10	75.05	37.52	1.47	85.30	br. w
7.00	163.30	156.30	78.15	39.08	1.42	85.15	v.w
5.20	165.00	159.80	79.90	39.95	1.39	85.10	med-w br
4.35	166.20	161.85	80.92	40.46	1.38	85.28	med

Table A.10. Laidlaw matrix.

LHS	RHS	4O	2O	O	d-sp	center	Intensity
92.15	112.85	20.70	10.35	5.17	9.92	102.50	
87.95	116.90	28.95	14.48	7.24	7.11	102.43	
87.00	118.10	31.10	15.55	7.77	6.62	102.55	
81.75	123.50	41.75	20.88	10.44	4.94	102.62	v.w.br
80.90	124.30	43.40	21.70	10.85	4.76	102.60	v.w
79.50	125.60	46.10	23.05	11.52	4.48	102.55	
78.20	126.85	48.65	24.32	12.16	4.25	102.52	
76.90	128.35	51.45	25.72	12.86	4.02	102.62	v.w
75.90	129.30	53.40	26.70	13.35	3.88	102.60	w
75.30	129.80	54.50	27.25	13.63	3.80	102.55	w
74.35	131.00	56.65	28.33	14.16	3.66	102.68	v.w
72.85	132.40	59.55	29.78	14.89	3.48	102.62	br.
71.45	133.65	62.20	31.10	15.55	3.34	102.55	100%
70.00	135.00	65.00	32.50	16.25	3.20	102.50	
67.80	137.50	69.70	34.85	17.42	2.99	102.65	b.
63.50	141.90	78.40	39.20	19.60	2.67	102.70	v.v.w
62.65	142.75	80.10	40.05	20.02	2.61	102.70	2 edges of br
61.60	143.75	82.15	41.08	20.54	2.55	102.68	str peak
60.65	144.55	83.90	41.95	20.98	2.50	102.60	v.w.
59.80	145.45	85.65	42.82	21.41	2.45	102.62	
59.20	146.00	86.80	43.40	21.70	2.42	102.60	v.w.
58.70	146.55	87.85	43.92	21.96	2.39	102.62	
57.80	147.55	89.75	44.88	22.44	2.35	102.68	
56.30	148.95	92.65	46.32	23.16	2.28	102.62	
55.35	149.95	94.60	47.30	23.65	2.23	102.65	
52.75	152.45	99.70	49.85	24.92	2.12	102.60	
50.05	155.10	105.05	52.52	26.26	2.02	102.57	3 lines
49.40	155.90	106.50	53.25	26.62	2.00	102.65	close
48.80	156.55	107.75	53.88	26.94	1.98	102.68	together
46.65	158.60	111.95	55.97	27.99	1.91	102.62	v.w
44.55	160.70	116.15	58.08	29.04	1.84	102.62	v.w.
43.60	161.65	118.05	59.03	29.51	1.82	102.62	str.
37.95	167.40	129.45	64.72	32.36	1.67	102.68	
37.40	168.00	130.60	65.30	32.65	1.66	102.70	v.w.
34.25	170.65	136.40	68.20	34.10	1.60	102.45	v.v.w.br
31.75	173.60	141.85	70.92	35.46	1.54	102.68	str.

29.65	175.70	146.05	73.02	36.51	1.50	102.67	
28.85	176.50	147.65	73.82	36.91	1.49	102.68	w.
26.80	178.55	151.75	75.88	37.94	1.46	102.68	
24.60	180.75	156.15	78.08	39.04	1.42	102.68	v.w.
22.00	183.35	161.35	80.68	40.34	1.38	102.68	
21.35	184.00	162.65	81.32	40.66	1.37	102.68	

IMAGE EVALUATION TEST TARGET (QA-3)

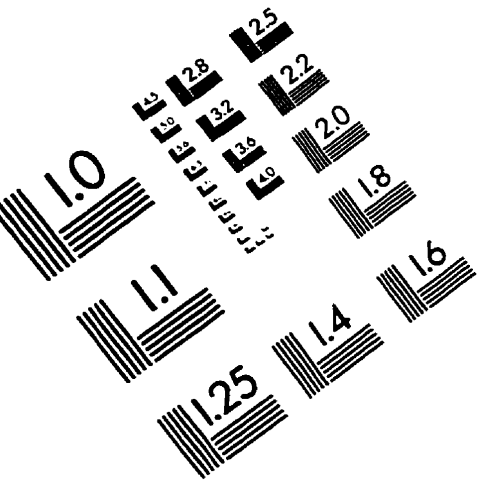

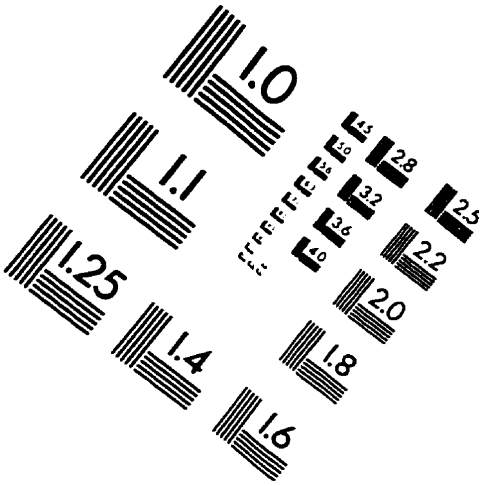

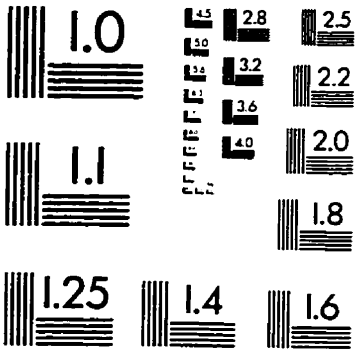

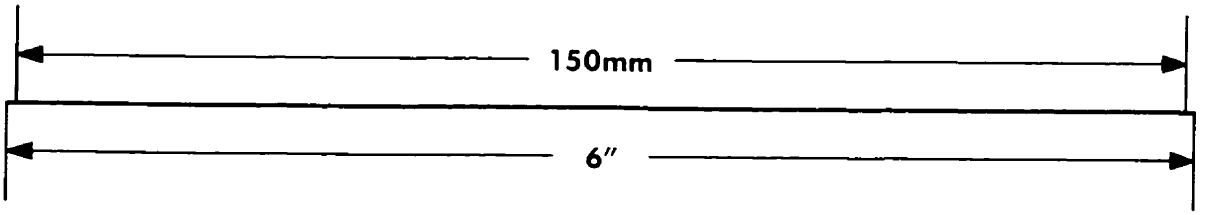

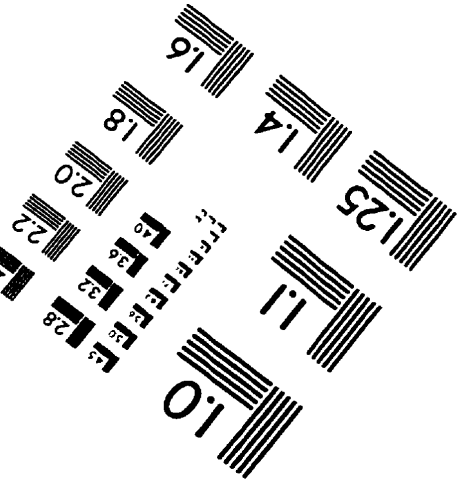

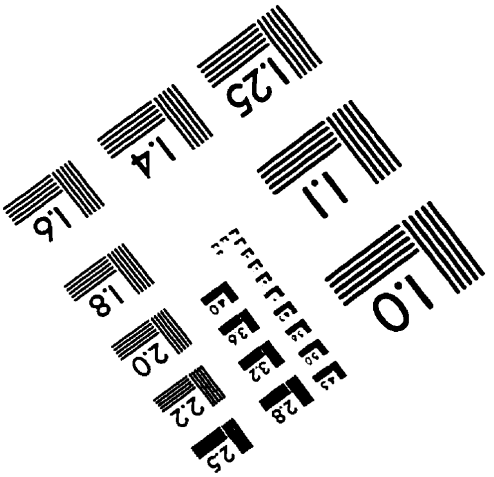

APPLIED IMAGE, Inc
1653 East Main Street
Rochester, NY 14609 USA
Phone: 716/482-0300
Fax: 716/288-5989